THE FOLLOWING PAGES WERE NOT

RECEIVED WITH ORIGINAL DOCUMENT AND

THEREFORE HAVE NOT BEEN REPRODUCED:

23

PUISQUE LES PAGES SUIVANTES N'ONT PAS ÉTÉ

REÇUES AVEC LE DOCUMENT ORIGINAL

ELLES N'ONT PAS ÉTÉ REPRODUITES:

PREDICTION OF COMBUSTION PERFORMANCE
OF
LOW VOLATILE GOODRICH COAL

A CONTRACT REPORT FOR

CANADA CERTRE FOR MINERAL AND ENERGY TECHNOLOGY,

CANADA

JUNE 1986

BY

DR F.C. LOCKWOOD AND DR S.M.A. RIZVI

DEPARTMENT OF MECHANICAL ENGINEERING

IMPERIAL COLLEGE OF SCIENCE AND TECHNOLOGY,LONDON

MICROMEDIA

108 pp

FILE REFERENCE : 02SQ.23440-4-9005

CONTRACT NO: 0SQ84-00026

IMPERIAL COLLEGE REFERENCE: 3A

ABSTRACT

The results of validation studies of a computational procedure are presented for a low volatile Canadian coal and for a high volatile one for two swirl numbers. The prediction procedure is that developed at Imperial College under a prior contract especailly concerned with high volatile Canadian coals. The data have been collected at Canadian Combustion Research Laboratories (CCRL) in a cylindrical furnace fired by a burner specially conceived to combust low volatile coal. Both the low volatile and high volatile data are reasonably well predicted. The physical modelling for the high volatile Coal Valley coal of this study was the same as that used for the Alberta coals of a prior study for the CCRL. This modelling had however to be altered to obtain satisfactory predictions for the low volatile Goodrich fuel of this study. The alterations comprised augmenting the quantity of particle material released as reducing the devolatilization kinetics rate and reducing the char chemical kinetic rate. With these modifications both the CCRL low volatile data sets for two swirl numbers were predicted without further adjustment of model parameters.

CONTENTS

ABSTRACT	i
CONTENTS	ii
List of Tables	v
List of Figures	vi
1. Introduction	1
2. Mathematical Formulation	5
2.1 Choice of Method for composit Phase	5
2.2.1. Governing Equations for Gas-Field	7
2.2.2. Turbulence Model	8
2.2.3. Final Form of the Equations for Gas-Phase	10
2.3 The Particulate Phase	12
2.3.1. Governing Equations for the Particulate Phase	13
2.3.2. Turbulent Dispersion Model	18
2.3.3. Final Form of Equations of Particle Motion	19
2.4 Radiative Heat Transfer Modelling	20
2.4.1. Non-Equilibrium Diffusion Radiation Model	21
3. Modelling of Particle and Volatile Reactions	27
3.1 Devolatilization	27
3.1.1. Devolatilization Scheme for High Volatile Coal	28
3.1.2. Devolatilization Scheme for Low Volatile Coal	29

3.2 Heterogeneous Char Combustion 30

3.2.1. Rate Limiting Processes 30
3.2.1a Chemical Kinetics 31
3.2.1b Mass transfer of oxygen to particle surface 32
3.2.1c Overall Rate coefficient 32
3.2.2. Combustion Modelling for High Volatile Coal 33
3.2.3. Combustion Modelling for Low Volatile Coal 34

3.3 Volatile Combustion Model. 35

4. The Numerical Procedure 36

4.1 The Specification of computing Grid and Layout of Variables 36

4.2 The Discretization Procedure 37

4.3 The Solution Algorithm 40

4.4 The PISO Algorithm 40

4.5 Handling of the Gas-Particle Interaction 44

4.5.1. Particle Tracking Procedure 46
4.5.2. Description of the Present Tracking Procedure 47
4.5.3. Summary of the Overall Tracking Procedure 49

4.6 Recurrence Relation solution Procedure for Particle Motion and Temperature 49

4.7 Computational Details 50

4.7.1. Overall solution Procedure 50
4.7.2. Under-relaxation Factors and Number of 'Sweeps' 51

5. Calculation Results 59

5.1 Geometry and Operating Conditions 59

5.2 The Experimental Data 59

5.3 Results and Discussion 60

5.3.1. High Volatile Coal 60
5.3.1a Swirl Setting 3.0, Flame 'CV1' 60
5.3.1b Swirl Setting 4.5, Flame 'CV2' 61
5.3.2. Low Volatile Coal 61
5.3.2a Swirl Setting 3.0, Flame 'GC1' 61
5.3.2b Swirl Setting 4.5, Flame 'GC2' 62

6. Concluding Remarks 93

REFERENCES 94

List of Tables

		Page
Table (2.1)	Model Constants for Two-Equation 'k"ε Turbulence Model and Related Turbulence Quantities	[illegible]
Table (2.2)	Radiation Properties of the Combustor and Combustion Gases	[illegible]
Table (4.1)	Expressions of Source Terms Appearing in the Governing Equations.	[illegible]
Table (4.2)	Residence Times and Source Expressions of Mass and Momentum in Tracking Technique	[illegible]
Table (4.3)	The Under-relaxation Factors and Number of sweeps	[illegible]
Table (5.1)	Specifications of the Coal used	64
Table (5.2)	Specifications of Basic Operating Conditions of the Flames Predicted	[illegible]
Table (5.3)	Particle size Ranges for the Flames	66

List of Figures

Fig. (4.1)	The Staggered Grid System	57
Fig. (4.2)	The Control Volumes (ϕ,U,V)	57
Fig. (4.3)	Particle Trajectory over a typical Portion of the Staggered Gird	58
Fig. (5.1)	Furnace Geometry and Computational Grid	67
Fig. (5.2)	CCRL Burner Geometry	68
Fig. (5.3a)	The Streak Lines pattern for the flame CV1 (Coal Valley Swirl setting = 3.0)	69
Fig. (5.3b)	Comparison of the predicted and measured gas temperature profiles at four downstream locations for Flame CV1 (Coal Valley, Swirl setting = 3.0)	70
Fig. (5.3c)	Comparison of the predicted and measured profiles of volume fraction of oxygen at four downstream locations for flame CV1 (Coal Valley, Swirl setting = 3.0)	71
Fig. (5.3d)	Comparison of the predicted and measured profiles of volume fraction of carbon dioxide at four downstream locations for flame CV1 (Coal Valley, Swirl setting = 3.0)	72
Fig. (5.3e)	Comparison of predicted and measured total heat transfer flux to the cooling walls for flame CV1 (Coal Valley, Swirl setting = 3.0)	73
Fig. (5.3f)	Comparison of predicted and measured incident radiation flux to the walls for flame CV1 (Coal Valley, Swirl setting = 3.0)	74

Fig. (5.4a) The streak lines pattern for the flame CV2 (Coal Valley, Swirl setting = 4.5) 75

Fig. (5.4b) Comparison of the predicted and measured gas temperature profiles at four downstream locations for Flame CV2 (Coal Valley, Swirl setting = 4.5) 76

Fig. (5.4c) Comparison of the predicted and measured profiles of volume fraction of oxygen at four downstream locations for Flame CV2 (Coal Valley, Swirl setting 4.5) 77

Fig. (5.4d) Comparison of the predicted and measured profiles of volume fraction of carbon dioxide at four downstream locations for flame CV2 (Coal Valley, Swirl setting = 4.5) 78

Fig. (5.4e) Comparison of predicted and measured total heat transfer flux to the cooling walls for flame CV2 (Coal Valley, Swirl setting 4.5) 79

Fig. (5.4f) Comparison of predicted and measured incident radiation flux to the walls for Flame CV2 (Coal Valley, Swirl setting = 4.5) 80

Fig. (5.5a) The streak lines pattern for the flame GC1 (Goodrich Coal, Swirl setting = 3.0) 81

Fig. (5.5b) Comparison of the predicted and measured gas temperature profiles at four downstream locations for Flame GC1 (Goodrich Coal, Swirl setting = 3.0) 82

Fig. (5.5c) Comparison of the predicted and measured profiles of volume fraction of oxygen at four downstream locations for flame GC1 (Goodrich Coal, Swirl setting = 3.0) 83

Fig. (5.5d) Comparison of the predicted and measured profiles of volume fraction of carbon dioxide at four downstream locations for Flame GC1 (Goodrich Coal, Swirl setting = 3.0) 84

Fig. (5.5e) Comparison of predicted and measured total heat transfer flux to the cooling walls for flame GC1 (Goodrich Coal, Swirl setting = 3.0) 85

Fig. (5.5f) Comparison of predicted and measured incident radiation flux to the walls for flame GC1 (Goodrich Coal, Swirl setting = 3.0) 86

Fig. (5.6a) The streak lines pattern for the Flame GC2 (Goodrich Coal, Swirl setting = 4.5) 87

Fig. (5.6b) Comparison of the predicted and measured gas temperature profiles at four downstream locations for Flame GC2 (Goodrich Coal, Swirl setting 4.5) 88

Fig. (5.6c) Comparison of the predicted and measured profiles of volume fraction of oxygen at four downstream locations for Flame GC2 (Goodrich Coal, Swirl setting = 4.5) 89

Fig. (5.6d) Comparison of the predicted and measured profiles of volume fraction of carbon dioxide at four downstream locations for Flame GC2 (Goodrich Coal, Swirl setting = 4.5) 90

Fig. (5.6e) Comparison of predicted and measured total heat transfer flux to the cooling walls for Flame GC2 (Goodrich Coal, Swirl setting = 4.5) 91

Fig. (5.6f) Comparison of predicted and measured incident radiation flux to the walls for Flame GC2 (Goodrich Coal, Swirl setting = 4.5) 92

1. Introduction

The main objective of the present research effort is the development of a cost-effective general prediction procedure for describing physical processing in a two-dimensional axisymmetric combustor using high-volatile (HVC) as well as low-volatile (LVC) pulverised coals. In the previous work undertaken by this research team sponsored by the Canada Centre for Mineral and Energy Technology (CANMET), a second generation prediction procedure was developed by introducing several new features into the first generation procedure making it more efficient and cost-effective, see Lockwood and Rizvi (1983), Lockwood and Rizvi (1984) and Rizvi (1985). The resulting procedure was applied to evaluate different models for physical processes critical for pulverised coal conversion reactions such as devolatilization and heterogeneous burning of the char particle. Four Alberta high volatile flames (HVF) have been successfully predicted by comparing calculation results with the measurements supplied by CANMET, see also Lockwood et al (1986).

The present study involves the application of the above calculation procedure to the low volatile flames (LVF) in order to assess the performance of the code and to improve it further to make it more versatile. The experimental data were obtained at the Canadian Combustion Research Laboratory (CCRL) of CANMET, Canada for the low/high volatile flames, see Hughes (1985). Calculations have been carried out for four swirling flames. Among these two are high volatile flames (coal valley, Canada) and the rest the low volatile (Goodrich, Canada) ones of different degrees of swirl. The specifications of the fuels and the flame input conditions may be found in Tables (5.1) and (5.2) respectively. The reason

for choosing the high volatile flame for prediction purposes again was that the burner geometry of the combustor had to be varied substantially from the previous case (Lockwood and Rizvi (1984)) due to the difficulties in firing low volatile coals.

The prediction procedure used here describes flow, combustion and heat transfer in turbulent swirling pulverised coal flames. The mathematical formulation applies the eulerian conservation equations for the gaseous carrier-phase. The particulate-phase is described in the lagrangian framwork where representative particle flights are tracked through the prevailing gas field using a tracking procedure. The particle motion and thermal balance equations are solved to obtain the particle histories of position, velocity and mass etc, as it travels through the combustor. The technique for handling the gas-particle interaction is termed the Particle Source In Cell (PSIC) method where the influence of the particle on the gas-phase is accountd for by source terms appended to the gas-phase conservation equations, see Migdal and Agosta (1967). An efficient and computationally economic particle tracking routine has been developed to solve for the particle trajectories using a novel 'recurrence relation type' solution scheme. A fast and cost-effective solution algorithm 'Pressure-Implicit-Split-Operator (PISO)' for the gas-phase calculations is introduced. A two-equation K~ϵ turbulence model is employed. For the gas-phase combustion a model is used which relates the rate of combustion to the rate of dissipation of eddies and expresses the rate of reaction in terms of the mean concentration of the reacting species, the turbulent kinetic energy and the rate of dissipation of this energy. For the radiation calculations, a 'non-equilibrium diffusion radiation model' is employed.

The recommended physical modelling and other optimized parameters suggested before (Rizvi (1985)) performed well for the high volatile flames in the present study. However, for the low volatile coals different model conditions and constants had to be used to obtain reasonable comparisons. One encouraging factor worth noting is the moderate degree of universality observed in the modelling and parameters in the calculations of low volatile flames.

A detailed survey of the literature available on the theoretical as well as the experimental studies regarding pulverised coal combustion and related subject may be found in Rizvi (1985) and need not be reviewed here. The research work on the studies of low volatile coal is scarce. Some noteworthy experimental work on the mechanism of heterogeneous combustion for LVC may be found in Field (1969), Field (1970), Smith (1971), Smith (1971^a), Hamor et al (1973) and Smith (1978). Theoretical studies specifically on the subject of low volatile coals are still scarcer. Wall et al (1986) presented one-dimensional predictions of the low volatile flames using measurements from AP11, AP12 and AP13 trials at International Flame Research Foundation (IFRF), see Phelan and Flament (1982), Phelan and Bortz (1983) and Phelan and Bortz (1985).

Generally, the results of the calculations in the present study for the HVF and LVF are satisfactory. The devolatilization and the char burn out models have been found to be important for the reasonable predictions of LVC. One particularly critical factor observed in the prediction of low volatile flames was the total amount of volatiles released, see sections (3.2.2.) and (5.3.2) for details. The combustion reaction close to the

symimetry axis are found to be under-predicted uniformly for all the four flames predicted here. The reason perhaps is in the approximation tothe real burner geometry due to the lack of data on the input velocity profiles. We have recently received some information regarding the input velocities (Hughes (1986)) but work on the question must now be deferred to the future.

2. Mathematical Formulation

2.1 Choice of Method for Composite Phase

There are two fundamentally different mathematical approaches to describe the flow situations in fluid motion: Eulerian and Lagrangian. In the Eulerian treatment the flow quantities are defined as functions of position in space and time. The Lagrangian description uses a material element of fluid and describes the flow field as a function of time and dynamical history of this element. The primary difficulty in modelling the particulate-gas mixture motion is that the Eulerian specification can conveniently describe the mathematical representation of the gas-phase, whereas Lagrangian description is suitable for discrete-phase, particularly the simulation of effects of drag, heat transfer and particle size etc.

The usual practice for two-phase motion modelling is to treat the carrier-phase as a continuum. One of the two approaches (Lagrangian or Eulerian) is applied to model the discrete-phase and the treatment of the phase coupling, i.e. the exchange of mass, momentum and energy between the phases.

Spalding (1971) using an Eurlerian approach, described the particle size distribution by a discretisation into uniform diameter groups with 'specieslike' partial differential equations being solved for the mass fraction of particles in each group. An Eulerian particle treatment of this kind was employed to make general computations in pulverised coal combustors by Gibson and Morgan (1970) and later by Gosman et al (1976). As expected, conceptual difficulties arise when the particulate phase is assumed to be a continuum in defining the averages for velocities and

temperatures. In the Lagrangian approach, formulated by Migdal and Agosta (1967) and later used by Crowe (1974) for a spray cooling problem, the flights of statistically reprsentative particles are tracked from the point of entry through to the combustor exit. The information regarding the presence of particles to the gas flow is provided by means of source coupling parameters of mass, momentum and energy.

Comparison studies between discrete and continuum models by Lockwood and Syed (1977) and by Abbas et al (1981) favour on the balance the Lagrangian approach against the Eulerian treatment. The following are considered to be the principal advantages which weigh in favour of Lagrangian treatment:

a) Particle slip is easily account for
b) The computer storage requirement does not increase with the number of size groups in contrast to the Eulerian approach. This may well be the single deciding factor for three-dimensional computations.
c) The particle behaviour like drag, heat transfer, devolatilization, char combustion and other physical laws are conveniently applied
d) The Lagrangian approach is computationally economical (see Abbas (1982))

Opposing the choice of the Lagrangian approach is the fact that turbulent dispersion of particles is less easily handled and that the Lagrangian based computations may be less stable because of the source terms imposed on the mean flow equations.

On the basis of the above arguments, we favour the Lagrangian treatment of the discrete phase for the present study.

2.2.1 Governing Equations for Gas-Field

Applying the Reynold's transport theorem for conservation of gaseous mass in a control volume of two-phase mixture, we obtain the gas-phase continuity equation:

$$\frac{\partial \rho}{\partial t} + \frac{\partial (\rho u_i)}{\partial X_i} = S_{p,m} \qquad (2.1)$$

where $S_{p,m}$ is the rate of mass added to the gas-phase per unit volume from the particle during mass removal by the devolatilization and combustion processes.

The momentum equation for the gas-phase in the composite mixture is obtained by applying the Reynold's transport theorem to the control volume enclosing gas-particle cloud and treating gas momentum as the transport property. The corresponding differential equation is written as

$$\frac{\partial (\rho u_j)}{\partial t} + \frac{\partial}{\partial X_i}(\rho u_i u_j) = - \frac{\partial p}{\partial X_i} + \frac{\partial \tau_{ij}}{\partial X_i} + S_{p_i} \qquad (2.2)$$

where S_{pi} is the momentum exchange rate between the particle and the gas-phases per unit volume.

The conservation of a scalar property ϕ can be obtained by applying the Reynold's transport theorem as before ϕ is a general scalar such as enthalpy or the species concentration. The particle-gas coupling will

again be via the exchange of the considered property ϕ between the phases obtained for the gas-phase. Taking ϕ as a general scalar such as enthalpy or the species concentration, the scalar transport equation is written as:

$$\frac{\partial}{\partial t}(\rho\phi) + \frac{\partial}{\partial X_i}(\rho u_i \phi) = \frac{\partial}{\partial X_i}(\Gamma_\phi \frac{\partial \phi}{\partial X_i}) + S_\phi \qquad (2.3)$$

where Γ_ϕ is the diffusion coefficient associated with the transport property ϕ and is assumed to be spatially invariant. S_ϕ is the source or sink of the scalar ϕ and is defined as

$$S_\phi = S_{g,\phi} + S_{p,\phi}$$

where $S_{g,\phi}$ is source or sink of ϕ associated entirely with the gas-phase and $S_{p,\phi}$ is the exchange of ϕ between the phases. Expressions for S_ϕ, $S_{g,\phi}$ are given in Table (4.1).

2.2.2 Turbulence Model

The two-equations 'k -ε' model has been favoured in the present case for the turbulence modelling. Its performance has been compared with the other available models (see Launder et al (1972)) and found to be surpassed only by more complex 'Reynold's stress' models. The 'k-ε' model is attractive because of its simplicity and generality. This model has been extensively used for non-reacting as well as the reacting recirculating and boundary-layer flows (see for example Launder et al (1972), Khalil et al (1976), Gosman et al (1976), Salooja (1978)).

The differential transport equation of turbulent kinetic energy K=1/2 $u'_i u'_i$ is derived by obtaining the equation for velocity fluctuation u'_i, multiplying it by u'_i and taking the time-average of the resulting equation (see Rodi (1970)). The transport equation for k may be written in the form:

$$\frac{\partial}{\partial t}(\rho k) + \frac{\partial}{\partial X_i}(\rho \bar{u}_i k) = \frac{\partial}{\partial X_i}\left(\frac{\mu_{eff}}{\sigma_k}\frac{\partial k}{\partial X_i}\right) + G - \rho\varepsilon \qquad (2.4)$$

where μ_{eff} and σ_k are effective viscosity and Prandtl number for turbulent energy respectively. G represents the generation of turbulent kinetic energy and is given by:

$$G = -\rho\overline{u'_i u'_j}\frac{\partial \bar{u}_i}{\partial X_j}$$

The effective viscosity, μeff is defined as μeff = $\mu+\mu_t$ where μ_t is the turbulent viscosity and μ is the molecular viscosity of the fluid. The transport equation for the dissipation rate of the turbulent kinetic energy is derived from a procedure similar to that of the k-equation. The equation takes the form:

$$\frac{\partial}{\partial t}(\rho\varepsilon) + \frac{\partial}{\partial X_i}(\rho \bar{u}_i \varepsilon) = \frac{\partial}{\partial X_i}\left(\frac{\mu_{eff}}{\sigma_\varepsilon}\frac{\partial \varepsilon}{\partial X_i}\right) + C_1\frac{\varepsilon}{k}G$$

$$- C_2 \rho \frac{\varepsilon^2}{k} \qquad (2.5)$$

where C_1 and C_2 are the model constant and σ_ε is Prandtl number for ε and of the order of unity. The model constants recommended by Launder and Spalding (1974) and Launder (1978) used for the present are listed in Table (2.1).

2.2.3 Final Form of the Equations for Gas-Phase

Time Averaged Continuity Equation

$$\frac{1}{r}\frac{\partial}{\partial r}(r\bar{\rho}\bar{v}) + \frac{\partial}{\partial z}(\bar{\rho}\bar{u}) = S_{p,m} \qquad (2.6)$$

Time-Averaged Form of the Momentum Equations

r-direction

$$\frac{1}{r}\left(\frac{\partial}{\partial r}(r\bar{\rho}\overline{vv}) + \frac{\partial}{\partial z}(r\bar{\rho}\overline{vu}\right) = \frac{1}{r}\left(\frac{\partial}{\partial r}(r\mu_{eff}\frac{\partial\bar{v}}{\partial r})\right.$$

$$\left. + \frac{\partial}{\partial z}(r\mu_{eff}\frac{\partial\bar{v}}{\partial z})\right) - \frac{\partial\bar{p}}{\partial r} + \bar{\rho}g_r + S_v + S_{p,v} \qquad (2.7)$$

z-direction

$$\frac{1}{r}\left(\frac{\partial}{\partial r}(r\bar{\rho}\overline{uv}) + \frac{\partial}{\partial z}(r\bar{\rho}\overline{uu})\right) = \frac{1}{r}\left(\frac{\partial}{\partial r}(r\mu_{eff}\frac{\partial\bar{u}}{\partial r})\right.$$

$$\left. + \frac{\partial}{\partial z}(r\mu_{eff}\frac{\partial\bar{u}}{\partial z})\right) - \frac{\partial\bar{p}}{\partial z} + \bar{\rho}g_z + S_u + S_{p,u} \qquad (2.8)$$

θ-direction

$$\frac{1}{r}\left(\frac{\partial}{\partial r}(r\bar{\rho}\overline{vw}) + \frac{\partial}{\partial z}(r\bar{\rho}\overline{uw})\right) = \frac{1}{r}\left(\frac{\partial}{\partial r}(r\mu_{eff}\frac{\partial\bar{w}}{\partial r})\right.$$

$$\left. + \frac{\partial}{\partial z}(r\mu_{eff}\frac{\partial\bar{w}}{\partial z})\right) + S_w + S_{p,w} \qquad (2.9)$$

where S_v, S_u and S_w are additional source terms associated with non-uniform viscosity, and $S_{p,v}$, $S_{p,u}$ and $S_{p,w}$ are sources to the gas-phase due to momentum exchange between the gas and particulate phase. A summary of the gas-phase source terms and the discrete-phase interaction source terms is also available in Table (4.1).

Time-Averaged Form of the Scalar Transport Equation

$$\frac{1}{r}\left(\frac{\partial}{\partial r}(r\bar{\rho}\bar{v}\bar{\phi}) + \frac{\partial}{\partial z}(r\bar{\rho}\bar{u}\bar{\phi})\right) = \frac{1}{r}\left(\frac{\partial}{\partial r}(r\Gamma_{\phi,eff}\frac{\partial\bar{\phi}}{\partial r})\right.$$

$$\left. + \frac{\partial}{\partial z}(r\Gamma_{\phi,eff}\frac{\partial\bar{\phi}}{\partial z})\right) + S_{\phi} \qquad (2.10)$$

where $\Gamma_{\phi,eff} = \frac{\mu}{\sigma_{\phi}} + \frac{\mu_t}{\sigma_{\phi,t}}$ and

(2.10b)

$$S_{\phi} = S_{g,\phi} + S_{p,\phi}$$

Transport Equation for the Turbulent Kinetic Energy 'k'

The transport equation for k, is written in the cylindrical co-ordinates for a steady axisymmetric flow as:

$$\frac{1}{r}\left(\frac{\partial}{\partial r}(r\bar{\rho}\bar{v}k) + \frac{\partial}{\partial z}(r\bar{\rho}\bar{u}k)\right) = \frac{1}{r}\left(\frac{\partial}{\partial r}(r\frac{\mu_{eff}}{\sigma_k}\frac{\partial k}{\partial r})\right.$$

$$\left. + \frac{\partial}{\partial z}(r\frac{\mu_{eff}}{\sigma_k}\frac{\partial k}{\partial z})\right) + G - \bar{\rho}\varepsilon \qquad (2.11)$$

Time-Averaged Form of the Transport Equation for the Rate of Dissipation of Kinetic Energy 'ε'

The time-averaged transport equation for the rate of dissipation 'ε' is written As

$$\frac{1}{r}\left(\frac{\partial}{\partial r}(r\bar{\rho}\bar{v}\varepsilon) + \frac{\partial}{\partial z}(r\bar{\rho}\bar{u}\varepsilon)\right) = \frac{1}{r}\left(\frac{\partial}{\partial r}\left(r\,\frac{\mu_{eff}}{\sigma_\varepsilon}\,\frac{\partial \varepsilon}{\partial r}\right)\right.$$

$$\left. + \frac{\partial}{\partial z}\left(r\,\frac{\mu_{eff}}{\sigma_\varepsilon}\,\frac{\partial \varepsilon}{\partial z}\right)\right) + C_1\,\frac{\varepsilon}{k}\,G - C_2\,\bar{\rho}\,\frac{\varepsilon^2}{k} \qquad (2.12)$$

The expression for G is available in Table (4.1).

2.3 The Particulate Phase

The discrete-particle model assumes that spherical shape particles, characterised by a certain size distribution, enter the computational region of the combustor from a finite number of representative locations in the plane of the burner exit. The particle size-distribution is assumed to consist of a finite number of size groups, each representing a certain number of mono-size identical particles having the same mass, momentum and temperature. The equations of conservation of mass, momentum and energy in the Lagrangian framwork are solved for each representative particle. The particulate and gas phases are coupled by feeding the local rates of mass, momentum and energy exchanges deduced from the particulate largrangian calculations to the Eulerian gas-phase equations.

2.3.1 Governing Equations for the Particulate Phase

The pulverized coal particle undergoes certain physical and chemical changes, upon entering the combustion space, due to the thermal exchange by mixing with the hot gases and due to the radiative absorption. This results in a loss of mass of the particle in the processes of devolatilization and the consecutive combustion of resulting char to ash. The rate of change of particle mass m_p, ignoring particle agglomeration or mass loss due to particle disintegration, can be written as:

$$- \frac{dm_p}{dt} = r_{e,p} \qquad (2.13)$$

where $r_{e,p}$ is the rate of mass efflux from the particle surface and depends upon whether the process is that of devolatilization or char combustion.

Particle Momentum Balance Equations

Using Newton's second law of motion for a non-rotating particle moving with a velocity $\underline{U}_p$ the sum of forces acting on the particle F, can be written as:

$$F = m_p \frac{d\vec{\underline{u}}_p}{dt} \qquad (2.14)$$

where force F is the resultant of the forces acting on the particle due to: the drag arising from the relative motion of the particle; the pressure gradient on the particle surface; gravitational effects, etc. The effect of all other forces can be ignored in comparison with the drag force which may be expressed as:

$$\vec{F}_d = C_D \rho \left(\frac{A_p}{2}\right) (\vec{u} - \vec{u}_p) . |\vec{u} - \vec{u}_p| \qquad (2.15)$$

where A_p is cross section area of the particle and C_D is the drag coefficient which depends upon the local particle Reynolds number. Using F_d for F in eq. (2.14) and writing the differential equations for the three particle velocity components we have:

$$\begin{aligned}
\frac{du_p}{dt} &= -\alpha \ (u_p - u) \\
\frac{dv_p}{dt} &= -\alpha \ (v_p - v) + \frac{w_p^2}{r_p} \qquad (2.16) \\
\frac{dw_p}{dt} &= -\alpha \ (w_p - w) - \frac{v_p w_p}{r_p}
\end{aligned}$$

where $\alpha = (18\mu C_D \, Re,p/24)/(\rho p d^2_p)$ and Re,p ρp and d_p are particle Reynolds number, density and its diameter. r_p is the distance of the particle from the axis.

Particle Energy Balance Equation

The total rate of heat gained or loss by the particle per unit mass, Q_t, is composed of the conributions of convection, Q_c, particle combustion, Q_b, and thermal radiation, Q_r. The total rate of heat intake to the particle per unit mass is thus:

$$Q_t = Q_c + Q_b + Q_r \tag{2.17}$$

In a situation where particle mass is changing due to devolatilization or combustion the rate of change of particle heat can be represented as:

$$\frac{d}{dt}(m_p C_p T_p) = m_p Q_t - C_p T_p(-\frac{d}{dt}m_p) - L_v\frac{dm_p}{dt} \tag{2.18}$$

where C_p is the particle specific heat, T_p is particle temperature and L_v is the latent heat of volatilization which is set to zero after devolatilization is complete.

Assuming $\frac{d}{dt} C_p = 0$, we have

$$C_p(\frac{dT_p}{dt}) = Q_t - \frac{L_v}{m_p}(\frac{d}{dt}m_p) \tag{2.19}$$

The above equation is used to calculate the particle temperature at discrete intervals in the combustor.

The rate of heat gain or loss per unit mass by the particle due to convection is (see also Baum and Street (1971)

$$Q_c = \pi\, d_p^2\, h\, (T_g - T_p)/m_p \qquad (2.20)$$

where h is the heat transfer coefficient and is given as

$$h = N_u \frac{K_G}{d_p}$$

where K_G is the thermal conductivity of the gas and N_u is the Nusselt number given by:

$$N_u = 2.0 + 0.6\, R_{e,p}^{1/2}\, P_r^{1/3}$$

where P_r is the Prandtl number.

We employ the following relation suggested by Baum and Street (1971) for the variation of the thermal conductivity of the combustion gas with temperature.

$$K_G = 6.739 \times 10^{-5} T_g + 6.446 \times 10^{-3}$$

The rate of heat liberated on or close to the surface of the particle due to char combustion is obtained by assuming that the reactions of carbon dioxide and water vapour with carbon are small and can be ignored. The particle rate of heat gain per unit mass due to burning is:

$$Q_b = \mu H_c \left(-\frac{dm_p}{dt}\right)/m_p \qquad (2.21)$$

where H_c is the char calorific value and μ is the fraction which estimates the amount of heat absorbed by the particle during combustion.

The rate of particle heat exchange due to radiation between the particle and the surroundings may be expressed as:

$$Q_r = \pi \sigma \varepsilon_p d_p^2 (T_R^4 - T_p^4)/m_p \qquad (2.22)$$

where σ is Stefan-Boltzmann constant (5.670×10^{-8} J/m^{2}s^{0}K^4), T_R is 'radiation temperature' and ϵ_p is the particle emissivity.

Particle Drag Law

For the present study we have employed the drag law due to Wallis (1969).

$$C_D = ((1 + 0.15\ R_{e,p}^{0.687})/\ R_{e,p}/24) \qquad (2.23)$$

The particle Reynolds number, $R_{e,p}$, is defined on the basis of particle relative velocity as:

$$R_{e,p} = \rho\ |\vec{u} - \vec{u}_p|\ d_p/\mu$$

2.3.2 Turbulent Dispersion Model

The expresssions for the particle 'drift velocity' to account for the turbulent dispersion of the particulate phase are given below. Further details on the subject are available in Lockwood and Syed (1977) and Lockwood et al (1980).

The particle diffusional velocities in the axial and radial directions are calculated from:

$$U_{diff} = C_1\sqrt{|\overline{u'^2}|}$$

and

$$V_{diff} = C_2\sqrt{|\overline{v'^2}|} \qquad (2.24)$$

where C_1 and C_2 are empirical constants. The gas velocity fluctuations in eq. (2.7.2) are calculated with the aid of the Boussinesq hypothesis:

$$\overline{u'^2} = - C_3 \, 2\frac{\mu_t}{\rho} \left(\frac{\partial \bar{u}}{\partial z}\right) + \frac{2}{3}k$$

$$\overline{v'^2} = - C_4 \, 2\frac{\mu_t}{\rho} \left(\frac{\partial \bar{v}}{\partial r}\right) + \frac{2}{3}k \qquad (2.25)$$

where C_3 and C_4 are further constants of the order of unity.

Using Eqs. (2.24) and (2.25) the particle drift velocities are written as

$$U_{diff} = C_1 \sqrt{\left| - C_3 \, 2\frac{\mu_t}{\rho} \left(\frac{\partial \bar{u}}{\partial z}\right) + \frac{2}{3}k \right|}$$

and

$$V_{diff} = C_2 \sqrt{\left| - C_4 \, 2\frac{\mu_t}{\rho} \left(\frac{\partial \bar{v}}{\partial r}\right) + \frac{2}{3}k \right|} \qquad (2.26)$$

the constants C_1 and C_2 are taken = 1.0.

2.3.3 Final Form of Equations of Particle Motion

Incorporating diffusional velocities to account for the particle dispersion, the equations of motion of the particle Eqs. (2.16) are modified to:

$$\frac{d\bar{u}_p}{dt} = -\alpha\{(\bar{u}_p + U_{diff}) - \bar{u}\}$$

$$\frac{d\bar{v}_p}{dt} = -\alpha\{(\bar{v}_p + V_{diff}) - \bar{v}\} + \frac{\bar{w}_p^2}{r_p}$$

$$\frac{d\bar{w}_p}{dt} = -\alpha\{(\bar{w}_p - \bar{w})\} - \frac{\bar{v}_p \bar{w}_p}{r_p} \qquad (2.27)$$

2.4. Radiative Heat Transfer Modelling

Radiation heat transfer plays a dominant role in most industry combustors and furnaces, especially oil or coal fired ones. The governing equation for the radiation exchanges are written in the form of a transport equation in terms of the radiation intensity I_λ, λ being the wavelengh of the monochromatic radiant energy. The radiation transport equation is written as:

$$(\underline{\Omega}.\nabla)\, I_\lambda = -(K_{\lambda a} + K_{\lambda s})\, I_\lambda + K_{\lambda a}\, I_{b\lambda} \qquad (2.28)$$

$$+ \frac{K_{\lambda s}}{4\pi} \int_{4\pi} p_\lambda(\underline{\Omega}, \underline{\Omega}') I_\lambda(\underline{\Omega}')\, d\omega'$$

Here $K_{\lambda a}$ and $K_{\lambda s}$ are the monochromatic absorption and scattering coefficients, $I_{b\lambda}$ is the intensity of black body radiation at wavelength λ. P_λ ($\underline{\Omega}$, $\underline{\Omega}'$) is the probability that incident radiation of wavelength λ in the direction $\underline{\Omega}'$ confined in the element of solid angle dw' will be scattered into the increment of solid angle dw in the incident radiation direction $\underline{\Omega}$. I_λ is defined as the amount of monochromatic radiant energy dQ transported in a given direction per unit area dA normal to the direction, per unit solid angle dw and per unit time dt:

$$I_\lambda \equiv \underset{d\lambda,\, dA,\, d\omega,\, dt \to 0}{\text{Lim}} \left(\frac{dQ}{d\lambda,\, dA,\, d\omega,\, dt}\right) \qquad (2.29)$$

2.4.1 Non-Equilibrium Diffusion Radiation Model

Gibb (1973) and Gibb (1977) proposed a simple and computationally economical radiation model which is an adaptation of non-equilibrium diffusion theory to suit the radiation calculations in furnaces: it is referred to as 'Non-Equilibrium Diffusion Radiation Model'. On the basis of simplicity, ease of application and computational economy, we have chosen the above model for the present radiation calculations.

The 'Non-Equilibrium Diffusion Radiation Model' is summarised as follows: To estimate the radiation behaviour approximately for a small volume in the combustion space, a single second-order elliptic equation of the following form is solved:

$$\nabla.(\frac{1}{3K_e}\nabla T_R^4) = (K_g + \bar{\varepsilon}_p K_p')T_R^4 - K_g T_g^4 - \bar{\varepsilon}_p K_p' \bar{T}_p^4 \qquad (2.30)$$

with the boundary conditions

$$-\frac{1}{3K_e}\frac{\partial T_R^4}{\partial n} = \frac{1}{2}\{(1-r_w)T_R^4 - \varepsilon_w T_w^4\}/(1+r_w) \qquad (2.31)$$

Here K_g is the gas absorption coefficient, T^4_p is the particle mean emission temperature, $\bar{a}_p K_p'$ is the total absorption coefficient for the particulate phase. γ_w and ϵ_w are the wall reflectivity and emissivity respectively and T_w is the wall temperature. K_e is the equivalent absorption coefficient defined as:

$$K_e = K_g + K_p'(\bar{\varepsilon}_p + \bar{r}_p(1-f)) \qquad (2.32)$$

where f is a 'scattering factor' given by:

$$f = \frac{1}{(4\pi)^2}\int_0^{4\pi} d\omega \int_0^{4\pi} p(\underline{\Omega},\underline{\Omega}')\ \underline{\Omega}.\underline{\Omega}'\ d\omega' \qquad (2.33)$$

The radiation flux may then be calculated as:

$$\underline{F}_R = - \frac{4}{3} \frac{\sigma}{k_e} \nabla T_R^4 \qquad (2.34)$$

The net gas and particle radiation absorption rates per unit volume, the estimates of the radiation energy sources to the gas energy balance equation can be expressed as:

$$S_{g,h} = 4 \sigma K_g (T_R^4 - T_g^4)$$

and

$$S_{p,h} = 4 \sigma \bar{\varepsilon}_p K'_p (T_R^4 - \bar{T}_p^4) \qquad (2.35)$$

Note that T_R^4 is all that is required from the present radiation model for the calculation of radiation sources $S_{g,h}$ and $S_{p,h}$ and it is obtained solving Eq. (2.30)

The radiation properties of the materials of the combustion chamber are required to be set within the combustion space and on the surface for radiation heat exchange calculations. Table (2.2) gives a summary of the constants used in the present study.

Table (2.1)

Model Constants for Two-Equation
'k~ε' Turbulence Model and
Related Turbulence Quantities

Constant	Value	Recommendations
c_μ	0.09	Launder and Spalding (1974)
C_1	1.44	
C_2	1.92	
σ_ε	1.3	
σ_k	0.9	Launder (1978)
σ_h	0.90	
$(\sigma_i)_{i=Vol,OX,P_r}$	0.90	

Table (2.2)

Radiation Properties of the Combustor and Combustion Gases

Property	Value
Absorption coefficient of the combustion gases, K_g	$0.1m^{-1}$
Absorption coefficient of soot, K_{soot}	$0.4m^{-1}$
Absorption coefficient of Particles, K_p	$\epsilon_p K_p'$ (K_p' is the cumulative projected area of particles of all sizes at all temperature in a small volume.)
Scattering coefficient of the particles, K_s	$(1-\epsilon_p) K_p'$
Emissivity of the Particles, ϵ_p	(X_{UB} + 0.6(1.0+X_{UB}) the fraction of the original char mass remaining unburnt at at any point.)
Scattering Factor, f	0.9
Wall emissivity, ϵ_w	0.5-0.7
Reflectivity of wall, r_w	$(1-\epsilon_w)$

3. Modelling of Particle and volatile Reactions

The mathematical modelling of the three major steps in p.f.(pulverised fuel) combustion: rapid pyrolysis; hetrogeneous combustion of resulting char particles and; gas-phase combustion of volatiles, are needed. The models describing the above processes are discussed below for the different fuels considered in the present study.

3.1 Devolatilization

When coal is heated to sufficiently high temperature it begins to decompose, producing tars and volatile matter. The volatiles consist of a mixture of combustible gases, carbon dioxide and water vapour. Char is the residual solid matter following devolatilization. The rate and extent of devolatization of coal particles play an important part in the processes occuring in a pulverised fuel flame.

It is generally accepted that the variables which influence significantly the pyrolysis process and the composition of the volatiles released are: coal dust type; concentration; particle size and size distribution. Also, the thermal history of the particles, including heating rate, final temperature, duration of heating, are essential, see for example Anthony and Howard (1976), Smoot and Pratt (1979) and Howard (1981).

It is well established that depending upon the coal type, the high heating rate and final particle temperatures yield an increasing amount of volatiles that can considerably exceed the amount observed during proximate

analysis (Field et al (1967), Eddinger et al (1966), Menstor et al (1974) and Anthony et al (1975)). Phelan and Bortz (1985) reported values of V^*/VM (V^*= the potential volatile yield and VM= ASTM volatile value of coal) from 1.5 for high volatile coals up to 2.5 for low volatile coals in their AP13 trials at International Flame Research Foundation. Wall et al (1986) used the experimental data of Phelan and Bortz (1985) to set the volatile yield for the prediction and scaling of burn-out in swirled pulverised coal flames. In the predictions of the high volatile flames Lockwood and Rizvi (1984) and Rizvi (1985) used a "Standard value" of V^*/VM as 1.2. The predictions of the low volatile coal flames in the presentstudy were found to be quite sensitive to V^*/VM is assumed to be 1.2 for high volatile coal (Coal Valley) and 2.0 for the low volatile coal (Goodrich coal). The different devolatilization models applied for the coal types are given below.

3.1.1 Devolatilization Scheme for High Volatile Coal

Following the recommendations of Lockwood and Rizvi (1984) and Rizvi (1985), the "Multiple Parallel Reactions Model" of Anthony and Howard (1976) is employed for the modelling of the high volatile coal flames in this study.

The volatile content V obtained in time t is expressed as (see Rizvi (1985)):

$$V = V^* \left(\sigma\sqrt{2\pi}\right)^{-1} \int_0^{\infty} \left(1 - \exp\left\{-\int_0^t K_o \exp(-E/RT)dt\right\}\right)$$

$$x \exp\left(-(E-E_o)^2/2\sigma^2\right) dE \qquad (3.1)$$

where Eo and σ are the mean value of the activation energy and the standard deviation of E. Ko is the pre-exponential factor of all the parallel reactions, T is the particle temperature and R is the gas constant. For the high volatile coals following values of the constants have been used.

$$V^* = 1.2VM \; ; \quad E_o = 2.12 \times 10^6 \text{ J/Kg mol}$$

$$K_o = 1.67 \times 10^{13} \text{ S}^{-1} \; ; \quad \sigma = 2.93 \times 10^7 \text{ J/Kg mol} \qquad (3.2)$$

3.1.2 Devolatilization Scheme for Low Volatile Coal

The devolatilization process for the low volatile Coal is modelled using the reaction rate expressed by single chemical decomposition reaction as (see Badzioch and Hawkesley (1970) for example):

$$\frac{dV}{dt} = K\,(V^* - V) \qquad (3.3)$$

where V is the cumulative amount of volatiles produced up to time t expressed as the weight fraction of the initial coal K is the rate constant given by Arrhenius expression as:

$$K=Ko \exp(-E/RT) \qquad (3.4)$$

For Goodrich coal (low volatile) the values: E= 0.65 x 10^8 J/kg mol, Ko=2.93x$10^4 s^{-1}$ and V^*=2.0 VM are used.

3.2 Heterogeneous Char Combustion

The char remaining after devolatilization consists primarily of Carbon, together with the major part of the ash components and some volatile matter. Heterogeneous gas-solid reactions involving a single char particle are governed by an intricate coupling of transport phenomena and chemical kinetics.

Historical aspects of coal and carbon combustion have been outlined by Essenhigh (1961) and Mulcahy (1978). Field (1967) and Smoot and Pratt (1979) have given comprehensive accounts of pulverised coal combustion. Specific reviews on the mechanics involved in the coal-oxygen and related reactions have been given by Thring and Essenhigh (1963), Mulcahy and Smith (1969), Essenhigh (1981). Smith (1982) reviewed factors controlling the reactivity of pulverised coal chars.

3.2.1. Rate Limiting Processes

The overall rate of char combustion is controlled by two rate limiting

processes: the chemical kinetic rate and the diffusion rate of oxidizer from the bulk gas to the particle surface.

3.2.1a Chemical Kinetics

The rate of reaction of a char particle with oxygen may be expressed as :

$$R_c = K_c (PO_2)_o^n \qquad (3.5)$$

where K_c is the chemical reaction rate coefficient of order n and $(PO_2)_0$ is the oxygen partial pressure at the surface. K_c may be expressed by an Arrhenius relation

$$K_c = A \exp (- E/RT)^n \qquad (3.6)$$

where A is the frequency factor and E is the apparent activation energy. T is the particle temperature. In general K_c combines the separate effects of the intrinsic reactivity of the carbon and the pore diffusion. Experimental studies have been carried out to determine the reaction rate coefficient K_c for different types of coals, see for example Field et al (1967), Field (1970). and Smith (1971).

3.2.1b Mass Transfer of Oxygen to Particle Surface

Mass balance considerations give the particle burning rate R_c as

$$R_c = K_d [(P_{O2}) \infty - (PO_2)_O] \qquad (3.7)$$

where $(PO_2)\infty$ is the oxygen partial pressure in bulk gas. Ka is the diffusion reaction rate coefficient given by (see Field et al (1967)):

$$K_d = D_c M_c \phi/[R d/2 (Tp + T_G)/2] \qquad (3.8)$$

Here D_c is the diffusion coefficient and is defined as:

$$D_c = D_o (\frac{Po}{p}) (\frac{TG}{To})^{1.75} \qquad (3.9)$$

where the subscript o designates reference temperature and pressure. D_o is the binary diffusion coefficient (m^2/s) for an O_2 - N_2 mixture M_c is the atomic weight of Carbon. ϕ is a mechanism factor and its value is 2 if CO is the main product and 1 if CO_2 is the main product being driven away from the particle boundary layer. T_p and T_g are the particle and gas temperatures respectively. D_o is taken as 3.13×10^{-4} m^2/s at reference temperature T_o= 1500°k and reference pressure $P_o = 1.013 \times 10^5$ N/m^2.

3.2.1c. Overall Rate Coefficient

Field et al (1967) recommended the use of an overall rate coefficient K_t, which is formed by combining the chemical rate coefficient K_c and the diffusion rate coefficient K_d. K_t is defined as:

$$K_t = 1/[(1/K_c) + (1/K_d)] \qquad (3.10)$$

It may be noted that when one of the terms (K_c or K_d) is much smaller than the other, the overall reaction is dominated by that term.

The char burning rate is written as:

$$\frac{dmp}{dt} = - K_t \bar{A}\, d^2\, p(FO_2)\, \infty \qquad (3.11)$$

where p is the gas pressure and $(FO_2)\,\infty$ is the molar fraction of oxygen in Combustion gas.

3.2.2. Combustion Modelling for High Volatile Coal

Lockwood and Rizvi (1984) and Rizvi (1985) made comprehensive studies to evaluate the experimental results (see Smith (1982)) for several high volatile bitumiuous coals of different origins. The constants A and E in Eq. (3.6) were optimized to predict three high volatile Alberta (Canada) flames. The optimized values of A and E in Eq. (3.6) (taking n=1)

$$A = 0.86 \text{ Kg} / \text{m}^2\text{s}/(\text{N}/\text{m}^2)$$

$$E = 1.02\text{x}10^8 \text{ J/Kg mol} \qquad (3.12)$$

The above model constants are employed to predict the high volatile coal valley flame.

3.2.3. Combustion Modelling for Low Volatile Coal

Wall et al (1986) has performed one-dimensional calculations for diverse coals including low volatile ones for experimental studies of AP11 trials (Phelan and Flament (1982)), AP12 trials (Phelan and Bortz (1983)) and AP13 trials (Phelan and Bortz (1985)) at International Flame Research Foundation.

In the present study for the low volatile coal the value of E in Eq. (3.6) is that recommended by Wall et al (1986). The pre-exponential factor A has been varied to obtain satisfactory comparisons following wall et al (1986).

Following are the values of A and E chosen for the low volatile flames:

$$A = 0.0086 \ Kg/m^2s/(N/m^2)$$
$$E = 0.071 \times 10^8 \ J/Kg\ mol \qquad (3.13)$$

3.3 Volatile Combustion Model

Magnussen and Hjertager (1976) proposed a simple and computationally economical combustion model using the 'eddy break-up' approach of Spalding (1971). The essential feature of this model is that it is applicable to premixed as well as diffusion flames. This model uses the standard two-equation 'k-ε' turbulence model. It is assumed that the turbulence decay rate, and so the reaction rate, is proportional to the time scale of the large-scale eddies as characterised by the ratio ε/k. Here k is the turbulent kinetic energy and ε is the dissipation rate of kinetic energy.

The model (Magnussen and Hjertager (1976)) further assumes that the reaction rate is proportional to the smallest of the fuel, oxygen, or products concentration. It follows that:

$$R_{fu} = \min\left(A\ \bar{\rho}\ \bar{m}_{fu}\ \varepsilon/k,\ \frac{A\bar{\rho}\bar{m}_{ox}}{S}\ \varepsilon/k,\ A'\ \bar{\rho}\ \frac{\bar{m}_{pr}}{(1+S)}\ \varepsilon/k\right) \qquad (3.14)$$

where R_{fu} is the volumetric reaction rate of fuel. ρ is the time averaged density, S is the stoichiometric oxygen requirement by mass. m_{fu}, m_{ox} and m_{pr} are respectively the time averaged mass, fractions of fuel, oxidant, and products, A,A' are empirical constants. The need for two constants instead of one shows the lack of universality of the model. This model has been termed as 'eddy dissipation combustion model'.

Following values of the constants A and A' are taken to model high and low volatile flames.

High Volatile flames: $A=4$, $A' =2$

Low Volatile flames: $A=8$, $A' =2$ (3.15)

4. The Numerical Procedure

The gas-phase differential equations presented in section 2 may be compactly written in the following form

$$\frac{\partial}{\partial x_i} (\rho \bar{u}_i \bar{\phi}) = \frac{\partial}{\partial x_i} (\Gamma_{\phi,eff} \frac{\partial \bar{\phi}}{\partial x_i}) + S_{g,\phi} + S_{p,\phi} \quad (4.1)$$

where $\bar{\phi}$ stands for the time-averaged value of any variable and $\Gamma_{\phi,eff}$ is the corresponding effective turbulent exchange coefficient defined by Eq. (2.10b). $S_{g,\phi}$ is a gas-phase source term for the eqation in question and $S_{p,\phi}$ is an additional source term due to gas particle interaction. A summary of the source terms appearing in Eq.(4.1) for each of the variables solved here is provided in Table (4.1).

4.1 The Specification of Computing Grid and Layout of Variables

Fig. (4.1) shows a staggered grid arrangement employed in the general algorithm for finite-difference computations, see Caretto et al (1972). The intersection of the solid lines denote the grid nodes where all the variable except $\bar{u}$ and $\bar{v}$ are stored and computed. The velocity components

are stored at points denoted by arrows (-) which are mid-way between the grid interactions. A node is denoted by P and its north, south, east and west neighbours by N, S, E and W respectively. The points, mid-way between P and its neighbouring nodes, lying along the boundaries of the P-cell, are denoted by n,s, e and w respectively, see Fig. (4.1). The control volumes (cell) for velocities and for other variables are shown in Fig. (4.2).

4.2 The Discretization Procedure

The discretized forms of the equations solved are obtained by the integration of the respective differential equations over the control volume pertaining to a particular variable. Integrating the differential equation, Eq. (4.1), over the volume V_p of a cell we get:

$$\Sigma\left\{ \int_A \left(\rho \bar{u}_i \bar{\phi} - \Gamma_{\phi,\text{eff}} \frac{\partial \bar{\phi}}{\partial X_i}\right)\right\} dA - \int_{V_p} S_{\phi T}\, dV = 0 \qquad (4.2)$$

where U_i and X_i are the time-averaged velocity and co-ordinate normal to the boundary and A is the area of the cell boundary under consideration. $S_{\phi,r}$ stands for the cumulative source effects per unit volume including those arising from the gas-particle interaction. The summation in Eq. (4.2) is over all the four boundaries of the cell.

Eq. (4.2) can be rewritten in the following form as:

$$-\dot{g}_w + \dot{g}_e - \dot{g}_s + \dot{g}_n - \int_{V_p} S_{\phi,T}\, dV = 0 \qquad (4.3)$$

where g_i (i=w,e,s,n) is the total convective and the diffusive flux of $\bar{\phi}$ transported across the boundary.

It has been shown (Gosman et al (1969)) that a good approximation with little loss of accuracy is obtained with the use of the 'hybrid' differencing formulation. The expression for the total flux passing through for example the west boundary using the hybrid differencing is given as:

$$\frac{\dot{g}_w}{(\rho \bar{u} A)_w} \equiv \begin{cases} \frac{1}{2}\{(1 + 2P_{e_w}^{-1})\bar{\phi}_W + (1 - 2P_{e_w}^{-1})\bar{\phi}_P\}, & \text{for } -2 < P_{e_w} < 2 \\ \bar{\phi}_W, & \text{for } P_{e_w} \geq 2 \\ \bar{\phi}_P, & \text{for } P_{e_w} \leq -2 \end{cases} \qquad (4.4)$$

here $P_{ew} = (\rho U)\, w\, \delta x/\Gamma_w$ is the local cell Peclet number.

The above hybrid scheme is equivalent to the 'upwind' differencing for high Peclet numbers and to the 'central' differencing scheme for low Peclet numbers, see Spalding (1972) and Runchal (1972) for details. The remaining fluxes, g_e, g_n and g_s in Eq. (4.3) are similarly evaluated.

The source term in Eq. (4.3) is split to take separate account for

sources due to gas-phase ($S_{g,\phi}$) and phase interaction ($S_{p,\phi}$). Thus:

$$\int_{V_p} S_{\phi,T}\, dV = S_{g,\phi} + S_{p,\phi} \qquad (4.5)$$

$S_{\phi,T}$ here denotes the production (generation) of the considered quantity $\bar{\phi}$ per unit volume. The gas-phase source term $S_{g,\phi}$ can be expressed as the linear function of $\bar{\phi}$:

$$S_{g,\phi} = S_u + S_p\bar{\phi} \qquad (4.6)$$

where S_u and S_p will in general be a function of $\bar{\phi}$.

Using the differencing scheme of Eq. (4.4) and the source term expressions of Eq. (4.6), the discretized finite-volume equation representing the parent differential equation Eq. (4.1) over the control volume becomes.

$$(a_p - S_p)\bar{\phi}_p = \sum_n a_n\bar{\phi}_n + S_u + S_{p,\phi} \qquad (4.7)$$

where $a_p = \sum_n a_n$

and $\sum_n a_n = a_W + a_E + a_N + a_S$; the summation over the neighbouring locations, W, E, N and S and $a_W = (\rho uAf)_w$ etc.

Also $\sum_n a_n\bar{\phi}_n = a_W\bar{\phi}_N + a_E\bar{\phi}_E + a_N\bar{\phi}_N + a_S\bar{\phi}_S$

4.3 The Solution Algorithm

The finite-volume equations (4.7) representing the differential equation (4.1) over the control volume surrounding each grid node for each variable yields a closed set of algebraic equations. These equations are easily solved by line-by-line (LBL) iterative solver employing the tri-diagonal matrix algorithm (TDMA) (see Patankar (1980) for example). The overall iterative procedure used here is the PISO (Pressure Implicit Split Operator) algorithm, developed recently at Imperial College, see Issa (1982) and Benodekar et al (1983). The PISO procedure replaces the slow SIMPLE (see Patankar and Spalding (1972) solution algorithm embodied in the original TEACH-T code. A brief outline of the PISO scheme is presented below.

4.4 The PISO Algorithm

The PISO procedure uses a two-stage predictor-corrector scheme, which, at each cylcle of iteration satisfies the mass and momentum balance equations more closely (than SIMPLE) and conseqently, improves the computational efficiency to a great extent. The PISO algorithm involves splitting of operations to deal with the coupling between velocity and pressure fields.

Let the superscripts, *, ** and *** denote intermediate field values obtained during the splitting operations.

The PISO procedure consists of the following sequential steps:

(a) Predictor Step The discretized finite-volume implicit momentum conservation equation refer to Eq. (4.7)) is written as:

$$a_p u_i = \sum_n a_n u_{in} - \Delta_i p + S_{u_i} \qquad (4.8)$$

where u_i stands for the velocity component U or V and Δ_i is the finite-difference equivalent of grad operating on the pressure p. S_{ui} is the cumulative associated source inclusive of the particle-gas interaction effects.

In this predictor step, the pressure field prevailing at m^{th} iteration, p^m, is used in the solution of Eq. (4.8) to obtain an intermediate velocity field u_i^*, thus:

$$a_p u_i^* = \sum_n a_n u_{in}^* - \Delta_i p^m + S_{u_i} \qquad (4.9)$$

(b) First Corrector Step A new velocity field u_i^{**} is sought together with a new pressure field p^* such that the divergence condition:

$$\nabla_i \, u_i^{**} = S_{p,m} \qquad (4.10)$$

representing the continuity is satisfied. For this situation the operative finite-volume momentum equation will be:

$$a_p u_i^{**} = \sum_n a_n u_{in}^{*} - \Delta_i p^{*} + S_{u_i} \qquad (4.11)$$

An incremental form of the momentum equation is obtained by subtracting Eq. (4.9) from Eq. (4.11) so that:

$$a_p (u_i^{**} - u_i^{*}) = - \Delta_i (p^{*} - p^{m}) \qquad (4.12)$$

Taking the divergence of Eq. (4.12) and using the continuity equation, we obtain the following form of the pressure-correction equation:

$$\nabla_i (a_p^{-1} \Delta_i)\, p' = \nabla_i u_i^{*} - S_{p,m} \qquad (4.13)$$

where $p' = p^{*} - p^{m}$

The pressure-correction equation (4.13) is solved in terms of p' and the first corrector stage velocity field u_i^{**} is calculated using Eq.(4.12)

(c) Second Corrector Step An improved velocity field u_i^{***} together with its corresponding pressure field p^{**} is obtained in the second corrector

step such that:

$$\nabla_i u_i^{***} = S_{p,m} \tag{4.14}$$

The operative momentum equation for this case is represented as:

$$a_p u_i^{***} = \sum_n a_n u_{i_n}^{**} - \Delta_i p^{**} + S_{u_i} \tag{4.15}$$

Subtracting Eq. (4.11) from Eq. (4.15) we get:

$$a_p (u_i^{***} - u_i^{**}) = \sum_n a_n (u_i^{**} - u_i^{*})_n - \Delta_i (p^{**} - p^{*}) \tag{4.16}$$

A second-stage pressure correction equation is obtained by combining the divergence of Eq. (4.16) with the continuity relations Eqs. (4.10) and (4.14). Thus:

$$\nabla_i \left(a_p^{-1} \Delta_i\right) p'' = \nabla_i \left(a_p^{-1} \sum_n a_n (u_i^{**} - u_i^{*})_n\right) \tag{4.17}$$

where $p'' = p^{**} - p^{*}$

Eq. (4.17) is solved for p" which is then used in conjunction with Eq.

(4.16) to calculate u_i^{***}. This completes the two-stage splitting operations resulting in the improved velocity field u_i^{***} and pressure field p^{**} for the $(m+1)^{th}$ iteration values, namely, u_i^{m+1} and p^{m+1}.

The above procedure is repeated in the given sequence until convergency is obtained, this is determined by examining the residual errors in each of the equation sets solved.

4.5 Handling of the Gas-Particle Interaction

The procedure for handling the gas-particle interaction is term the particle source in cell (PSIC) technique and was originally proposed by Migdal and Agosta (1967). This method has since been extensively used for various particulate research problems, see for example Lockwood et al (1980), Abbas (1982) and Lockwood et al (1984).

The presence of a coal particle in the finite-difference control volume (cell) of the gas-phase is made known through the application of source terms to the mean flow equations. As a coal particle enters the combustion space of a furnace it undergoes processes like devolatilization and burning resulting in exchange of mass between the two phases. The exchanges of momentum and energy between the two phases also occur due to the particle drag and the gas/particle convective and radiative heat transfer. The PSIC model for the gas-phase results in a mass source being appended to the gas-phase continuity equation; the drag force on the particle is reflected in the gas-phase calculations as a source of momentum; heat transfer between the particle and gas is identified bys an

enthalpy source while particle burning also results in sources being applied to the species conservation equations.

By the way of illustration, we may write the mass conservation equation for a control volume surrounding a grid node as:

$$- \dot{m}_w + \dot{m}_e - \dot{m}_s + \dot{m}_n - \Delta\dot{m}_p = 0 \qquad (4.18)$$

where $\dot{m}_w$, $\dot{m}_e$, etc. are the gas mass flow rates across for representation, the 'west', 'east', etc. faces of the control volume and $\Delta\dot{m}_p$ is the net mass efflux rate of coal particles in the gas-phase into the above control volume.

Similarly, considering the conservation of any property Φ over the control volume, we may write:

$$- F_w^{\Phi} + F_e^{\Phi} - F_s^{\Phi} + F_n^{\Phi} - \Delta F_p^{\Phi} = S^{\Phi} \qquad (4.19)$$

where F's represent the resulting convective and diffusive fluxes across each of the control volume boundaries and S^{Φ} is the conventional source term for the gas flow equation ($S^{\Phi} = S_{g,\Phi}$) such as radiation heat transfer and heat addition due to volatile combustion when Φ represents enthalpy. $\Delta F^{\Phi}{}_p$ is the net efflux of Φ into the gas-phase due to the particles. Again, for Φ representing the gas-phase enthalpy, $\Delta F^{\Phi}{}_p$ may stand for a positive particulate energy source for a burning particle and a negative source for a

particle receiving heat from hot gases.

The gas-particle interaction calculation scheme is iterative and entails the following principal steps in sequence:

(i) the computation of the gas-phase flow equations in the absence of the particulate-phase and for guessed initial values of the ϕ's

(ii) the calculation of the particle trajectories using the prevailing gas velocities

(iii) the calculation of the particle source terms i.e. the ΔF^{ϕ}_{p}'s for each control volume

(iv) the recomputation of the gas-field under the influence of particle source terms

(v) the last three steps are repeated until the convergence for all the equations being solved is achieved.

4.5.1 Particle Tracking Procedure

A new particle tracking technique is developed and included in the present prediction procedure. This has resulted in a major improvement in economy for equivalent accuracy, see Lockwood and Rizvi (1983). In the present tracking procedure the successive particle locations are obtained by a non-iterative method as in Lockwood et al (1980). In addition, to make

the tracking faster, the incremental time step Δt is chosen such that the corresponding spatial increment of the order of typical local cell dimensions is obtained. A brief description of the present tracking procedure is presented below.

4.5.2 Description of the Present Tracking Procedure

In Fig. (4.3) a particle trajectory between the two successive particle locations k and k+1 is superimposed on a typical portion of the staggered grid. The particle moves between position k and k+1, the distance increment of the order of the local cell dimensions in the time increment Δt_k. Position k is with reference to the scalar cell ϕ (I,J) (ϕ cell belonging to I^{th} vertical grid line and J^{th} horizontal grid line), the gas radial velocity cell V(I,J) and axial velocity cell U (I, J) on the computation mesh. The grid locations for the particle at position k+1 are: scalar cell ϕ (I, J+1); radial velocity cell V(I, J+1); and axial velocity cell U(I+1, J+1). The k^{th} time step Δt_k in such a situation is estimated as:

$$\Delta t_k = \min \left(\frac{\Delta X}{\bar{u}_{p,k}} , \frac{\Delta r}{\bar{v}_{p,k}} \right) \qquad (4.20)$$

where $\bar{u}_{p,k}$ and $\bar{v}_{p,k}$ are respectively the particle velocities in the X and r directions at position k and ΔX and Δr are the cell dimensions, see Fig. (4.3). The particle residence time between positions k and k+1 during visits of various cells is summarized in Table (4.2). Here Δt_1, Δt_2, etc. are the times spent by the particle between position k and A, positions A and B, etc. A uniform particle velocity between position k and k+1 is assumed.

The expressions for the sources of mass and momentum, apportioned to various cells visited by the particle in its displacement from the original position k to k+1, are presented in Table (4.2). Here δ_{mp} is the particle mass source to the gas-phase and $\delta M_{u,p}$ and $\delta m_{v,p}$ are the particle sources of momentum for the U and V velocity fields respectively when the particle moves from k to k+1. Similar expressions for the source terms for the other variables may be obtained.

4.5.3 Summary of the Overall Tracking Procedure

The numerical procedure for the particle tracking and particulate-phase calculations is summarized as follows:

(i) Using Eq. (4.20) estimate the time increment Δ_t ensuring that it corresponds to a distance increment for the particle equal to about the local cell dimensions.

(ii) Using this time increment Δt, and the gas-field conditions at position k, the particle-field equations of motion, Eqs. (2.27) and the particle energy conservation equation (2.19) are solved to obtain the next particle position k+1 and the particle temperature there.

(iii) Calculate time sub-steps Δt_1, Δt_2, etc., see Table (4.2), for every cell boundary intersection with the particle trajectory. Estimate, the resulting particle-interaction sources to the gas-phase computing cells, see Tables (4.1) and (4.2).

(iv) Repeat steps (i) to (iii) from the entry to the exit of the particle through the computing space.

(v) Steps (i) through (iv) are repeated so that all the representative particle sizes from all the starting locations are covered.

(vi) The cumulative phase-interaction sources are collected for every cell in the domain of computation.

4.6 Recurrence Relation Solution Procedure for Particle Motion and Temperature

A fast and relatively stable calculation procedure similar to that used by Lockwood and Shah (1981) for the solution of the radiation transport equation, is employed here for the solution of the particle motion equations (2.27) and the particle temperature equation (2.19)

All the above equations can be expressed in the following general form:

$$\frac{d\xi}{dt} = A - B\xi \qquad (4.21)$$

where expressions for A and B for the case of the temperature equation (2.19) are given as:

$$A = k_1 T_g + k_2 + k_3 T_R^4$$

$$B = k_1 + k_3 T_p^3 \qquad (4.22)$$

and where k_1, k_2 and k_3 are further defined as:

$$k_1 = \pi N_u K_G d_p/(m_p C_p)$$
$$k_2 = \{-\eta H_c(\frac{dm_p}{dt}) + (1-\eta)L_v\}/(m_p C_p)$$
$$k_3 = \pi c \varepsilon_p d_p^2/(m_p C_p) \qquad (4.23)$$

Assuming constancy of the coefficients A and B over a time increment δt, a recurrence relation of the follwing form can be obtained from solving Eq. (4.21):

$$\xi_{k+1} = \xi_k e^{-B\delta t} + (A/B)(1 - e^{-B\delta t}) \qquad (4.24)$$

where locations k and k+1 are at the beginning and end of the time increment. This procedure has resulted in particularly fast and stable computations, see Lockwood and Rizvi (1983) and Lockwood et al (1984).

4.7 Computational Details

Some relevant details of the computing procedure such as overall solution method, under-relaxtion factors, etc., are presented in this section.

4.7.1 Overall Solution Procedure

The overall solution procedure for the set of the finite-volume equations obtained for all the dependent variables proceeds iteratively as follows:

1. An initial guess is made for all the variables solved.

2. The finite-volume equations of the axial and radial velocity components are solved using an assumed pressure field.

3. The velocity field calculated in Step (2) is corrected using PISO algorithm and an improved pressure field obtained.

4. The tangential velocity equation is solved.

5. Using the current U, V and W field, the turbulence energy and dissipation rate equations are solved and improved viscosity is obtained.

6. The particle-field equations are solved using the gas-field obtained in Steps (3) and (4) to obtain particle trajectories and time-temperature histories etc. The gas-particle interaction source terms are then calculated for each control volume.

7. The enthalpy, radiation and rest of the species conseration equations are solved. The other auxiliary quantities such as gas density and gas temperature etc. are obtained.

8. Steps (2) to (6) are repeated until the convergence is achieved.

4.7.2 Under-relaxation Factors and Number of 'Swoeps'

Using α as the under-relaxation factor and ϕ_{new} and ϕ_{old} as the variable values obtained at the end of the current iteration and an

iteration before, the under-relaxed variable value $\bar{\phi}$ is given as:

$$\bar{\phi} = \alpha \, \bar{\phi}_{old} + (1 - \alpha) \, \bar{\phi}_{new}$$

The under-relaxation factor used in the present study is specified for each variable in Table (4.3).

In the line-by-line (LBL) solution procedure of a set of difference equations, the solution is generated along a chosen line by tri-diagonal matrix algorithm (TDMA) and then the entire grid is swept through, and as many 'sweeps' as necessary may be employed. The number of sweeps used in the prediction procedure for different variables is given in Table (4.3).

Table (4.1)

Expressions of Source Terms Appearing in the Governing Equations

Variable $\bar{\phi}$	$S_{g,\phi}$ (To be multiplied by V_p)	$S_{p,\phi}$
$\bar{u}$	$\frac{1}{r}\frac{\partial}{\partial r}(r\mu_{eff}\frac{\partial \bar{v}}{\partial z}) + \frac{\partial}{\partial z}(\mu_{eff}\frac{\partial \bar{u}}{\partial z}) - \frac{\partial p}{\partial z} - \frac{\partial}{\partial z}(\frac{2}{3}\bar{\rho}k)$	$\sum_{N}\sum_{L}\sum_{M} - \left\{\{(\dot{m}_p\bar{u}_p)_{k+1} - (\dot{m}_p\bar{u}_p)_k\}_M \frac{\delta t_{k,M}}{\Delta t_{k,M}}\right)_{L,N}$
$\bar{v}$	$\frac{1}{r}\frac{\partial}{\partial r}(r\mu_{eff}\frac{\partial \bar{v}}{\partial r}) + \frac{\partial}{\partial z}(\mu_{eff}\frac{\partial \bar{u}}{\partial r}) - \frac{\partial p}{\partial r} + \frac{\rho\bar{w}^2}{r}$ $- 2\mu_{eff}\frac{\bar{v}}{r^2} - \frac{\partial}{\partial r}(\frac{2}{3}\bar{\rho}k)$	$\sum_{N}\sum_{L}\sum_{M} - \left\{\{(\dot{m}_p\bar{v}_p)_{k+1} - (\dot{m}_p\bar{v}_p)_k\}_M \frac{\delta t_{k,M}}{\Delta t_{k,M}}\right)_{L,N}$
$\bar{w}$	$-\{\frac{\mu_{eff}}{r^2} + \frac{\rho\bar{v}}{r} + \frac{1}{r}\frac{\partial \mu_{eff}}{\partial r}\}\bar{w}$	$\sum_{N}\sum_{L}\sum_{M} - \left\{\{(\dot{m}_p\bar{w}_p)_{k+1} - (\dot{m}_p\bar{w}_p)_k\}_M \frac{\delta t_{k,M}}{\Delta t_{k,M}}\right)_{L\ N}$
k	$G - \rho\,\varepsilon$ (Eq. (2.5.11) for G)	0

cont'd...

Variable $\bar{\phi}$	$S_{g,\phi}$ (To be multiplied by V_p)	$S_{p,\phi}$
ε	$\{C_1 G - C_2 \rho \varepsilon\}\varepsilon/k$	0
$\bar{h}$	$R_{fu} H_v + 4\sigma k_g (T_R^4 - T^4)$ (H_v is the heat released by volatiles per unit mass)	$S_{p,h_1} + S_{p,h_2}$ (Eq. (4.7.7) for S_{p,h_1} & Eq. (4.7.8) for S_{p,h_2})
Rad	$- K_g (T_R^4 - T^4)$	$- V_p \sum_{N} \sum_{L} \sum_{M} \{\frac{n\pi d^2}{4V_p} \varepsilon_p (T_R^4 - T_p^4) \delta_{k,M}\}_{L,N}$
Vol	$- R_{fu}$	$(1 - \eta) S_{p,m}$ (Eq. (4.7.4) for $S_{p,m}$)
O_2	$- R_{fu} . S_v$ (S_v is the oxygen required to burn 1 kg of volatiles)	$- \frac{32}{12} \eta S_{p,m}$
P_r	$R_{fu} . P_v$ (P_v is the product formed by burning 1 kg of volatiles)	$\frac{44}{12} \eta S_{p,m}$

Table (4.2)

Residence Times and Source Expressions of
Mass & Momentum in Tracking Technique (see Fig. (4.3))

Cell Identification	Residence Time	Source Type	Source Value
$\phi(I, J)$	$(\Delta t_1 + \Delta t_2 + \Delta t_3)$	Mass	$\left(\frac{\Delta t_1+\Delta t_2+\Delta t_3}{\Delta t_k}\right) \delta m_p$
$\phi(I,J+1)$	Δt_4	Mass	$(\Delta t_4/\Delta t_k)\ \delta m_p$
$V(I,J)$	Δt_1	V-Momentum	$(\Delta t_1/\Delta t_k)\ \delta M_{v,p}$
$V(I, J+1)$	$(\Delta t_2 + \Delta t_3 + \Delta t_4)$	V-Momentum	$\left(\frac{\Delta t_2+\Delta t_3+\Delta t_4}{\Delta t_k}\right) \delta M_{v,p}$
$U(I,J)$	$(\Delta t_1 + \Delta t_2)$	U-Momentum	$(\Delta t_1 + \Delta t_2)/\Delta t_k\ \delta M_{u,p}$
$U(I+1, J)$	Δt_3	U-Momentum	$\Delta t_3/\Delta t_k\ \delta M_{u,p}$
$U(I+1, J+1)$	Δt_4	U-Momentum	$\Delta t_4/\Delta t_k\ \delta M_{u,p}$

Table (4.3)

The Under-relaxation Factors and Number of Sweeps

Variable	Under-relaxation factor α		No. of sweeps NSW	
$\bar{u}$, $\bar{v}$ and $\bar{w}$-velocity	0.7		2	
Pressure correction	1.0		not fixed	
Kinetic energy & dissipation rate	0.7		1	
Enthalpy	0.7		1	
Species concentrations	0.7		1	
Volatile concentration	0.2		1	
Radiation equation	1.0		1	
Density	0.4		-	
Viscosity	1.0		-	
Particle source	0.4		-	

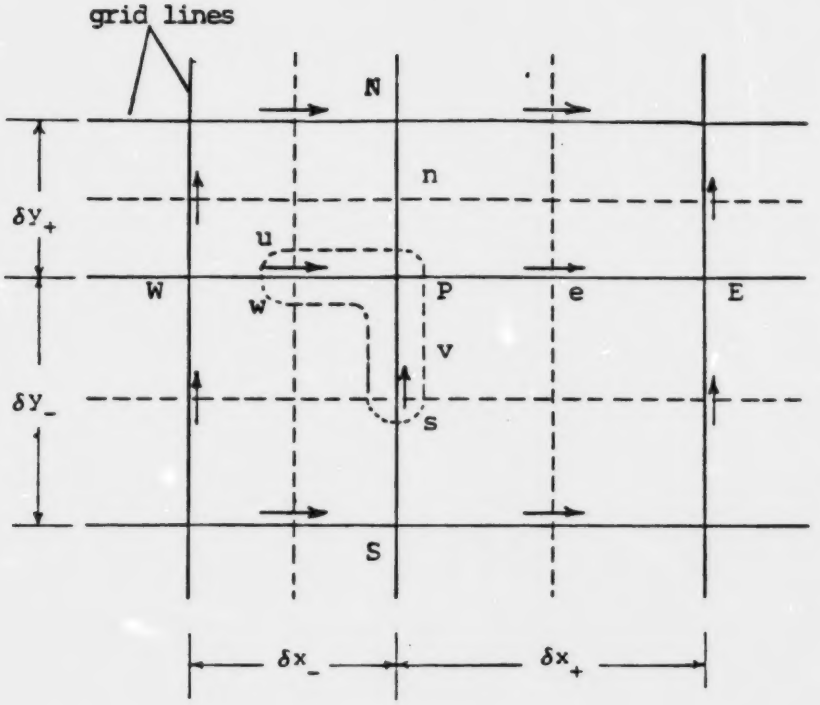

Fig.(4.1) The staggered Grid System

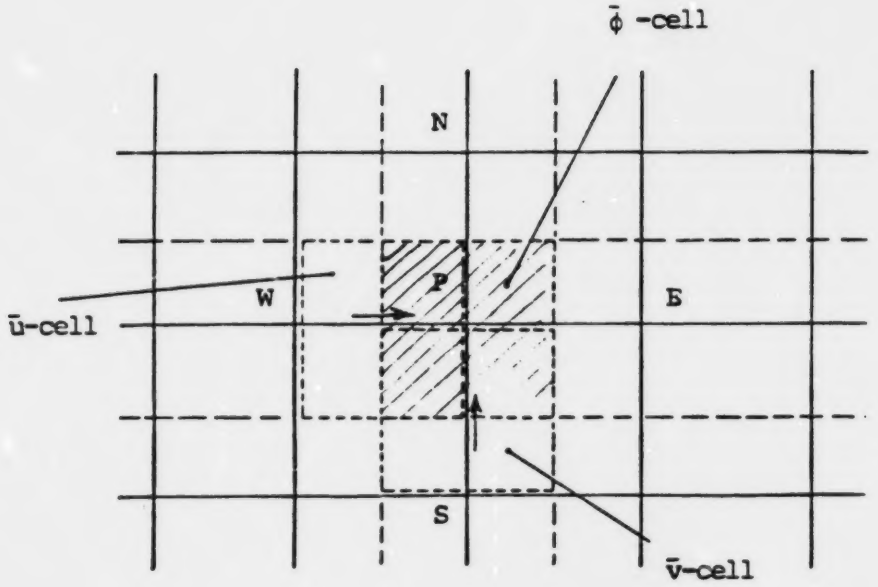

Fig.(4.2) The Control Volumes ($\bar{\phi}$, $\bar{u}$, $\bar{v}$)

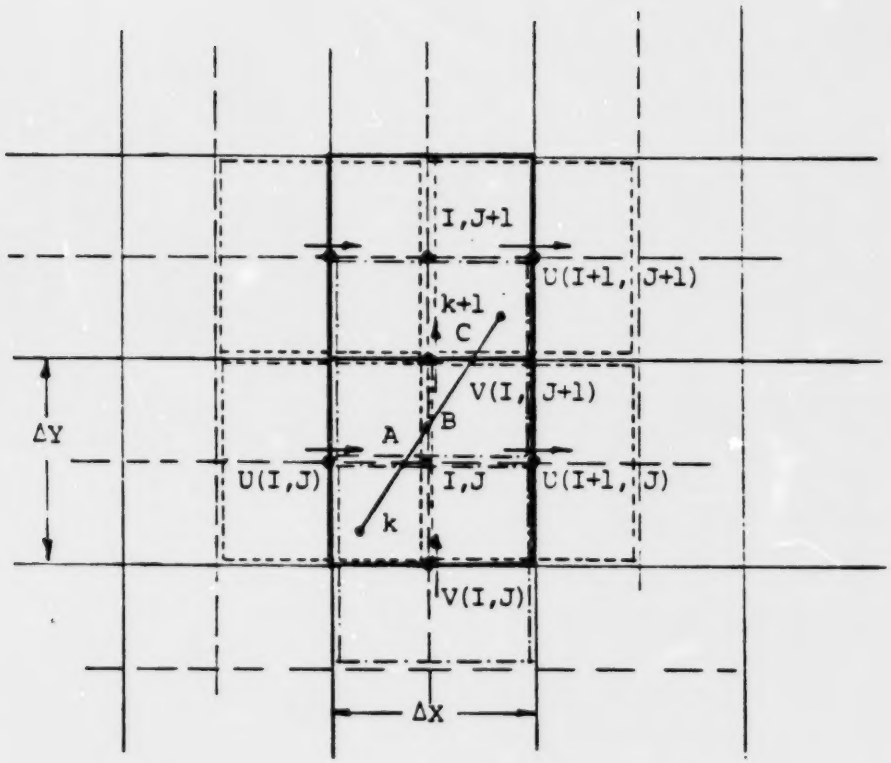

Fig. (4.3) Particle Trajectory Over a Typical Portion of the Staggered Grid

5. Calculation Results

5.1 Geometry and Operating Conditions

The combustor geometry and computational grid are sketched in Fig (5.1). This furnace is a 1m diameter cylinder axially fired from one end by a double concentre burner. A cone shaped bluff body is used in front of the burner to stabilize the flame. A quarl of 25^{o} half angle is employed. An initial 1m length of the cylindrical wall is refractory lined, the remaining length being cooled by an organic fluid. A computational grid of (51x37) is used for finite difference calculations.

Predictions have been obtained for the two coals specified in Table (5.1) in which one, the Coal Valley coal is a high volatile coal while Goodrich is a low volatile one. Flames with two swirl settings were predicted for the above two coals. The furnance operating conditions for the four flames code named CV1, CV2 (high volatile) and GC1, GC2 (low volatile) are presented in Table (5.2). Table (5.3) gives the particle size ranges used for the above flames.

5.2 The Experimental Data

The experimental data used here are those obtained for the low volatile bituminous coal flames for the tunnel furnance at the Canadian Combustion Reserach Laboratory (CCRL) of the Canada Centre of Mineral and Energy Technology (CANMET), Canada in March-May 1985, see Hughes (1985).

The main objective of these exeriments was to evaluate and improve the predictive capabilities of the prediction procedure developed earlier (see Lockwood and Rizvi (1984) Rizvi (1985)) for the CCRL data for the high volatile pulverised coal flames. The two sets of data points observed for each flame (see Figs (5.3) for example) are because of asymmetry in the combustor due to gavity. We of course have modelled the furnace axi-symmetric.

5.3. Results and Discussion

It is to be noted here that the burner geometry of the CCRL Combustor used to obtain the present data is markedly different from the previous case which have been used in Lockwood and Rizvi (1983) and Lockwood and Rizvi (1984). The burner used here is sketched in Fig (5.2). For this reason it was thought essential to monitor the performance of the prediction procedure for a high volatile coal first for low volatile which this code has been set up. Later the results were obtained for low volatile Goodrich coal. The low volatile flames could only be predicted by using different model condtions and other parameters. Two swirling flames of swirl setting 3.0 and 4.5 are predicted for each coal type. The lower swirl setting 3.0 is equivalent to swirl number of 0.5 and high swirl setting of 4.5 gives swirl number = 0.75, see McAskill and Hallett (1984). The results of the calculation for the above flames are presented below.

5.3.1. High Volatile Coal

5.3.1a Swirl Setting 3.0, Flame 'C1'

Results of the calculation for the low swirl setting are displayed in Figs (5.3). The aerodynamic behaviour of this flame near the burner region is presented in from of the streak lines pattern in Fig. (5.3a). Three recirculation zones A,B and C may be seen. The recirculation zone A is due to the conical bluff body placed in front of the primary stream. The second recirculation zone B inside the sleeve is due to the entrainment of the slower secondary stream into the faster primary stream and also due to the sudden expansion in the sleeve region. The third recirculation zone C is the largest among the three penetrating into the quarl zone and is called 'external recirculation region'. The general behaviour of this flame is expected to be the same as the type O flame of the recent IRFR flame classification system, see Hagiwara et al (1986).

Radial gas temperature profiles at four downstream furnace locations are presented in Fig. (5.3b). The predictions compare well with the experimental data except for the location nearest to the burner in the neighbourhood of the axis. This discrepency is also reflected in Figs

(5.3c) and (5.3d) for the oxygen and carbon dioxide concentration respectively. Fig (5.3e) gives the comparison of the predicted heat flux absorbed by the cooling system against the measurements for the flame CV1. The predicted incident radiation flux reaching the wall is compared in Fig. (5.3f). The quality of the heat transfer predictions was are good as in the previous case (Lockwood and Rizvi (1984)).

5.3.1.b Swirl setting 4.5, Flame 'CV2'

The streak lines pattern for the flame with a high swirl setting of 4.5 (swirl number = 0.75, Flame CV2) is given in Fig.(5.4a). Contrary to the expectations no 'internal' or 'central' recirculation zone is developed in the flame. The reason appears to be the high primary/total mass flow ratio of ≈60% and primary/secondary momentum ratio of ≈8.0 . Similar to the previous flame, CV1, the CV2 flame is also of type O and so exhibits similar behaviour. Fig. (5.4b) displays the radial gas temperature profiles. Concentration profiles for the oxygen and Carbon dioxide may be found in Figs. (5.4c) and (5.4d) respectively. The heat transfer from the flame to the combustor wall is presented in Figs (5.4e) and (5.4f). Generally, the quality of the predictions for both the high volatile flames CV1 and CV2 is about the same.

5.3.2. Low Volatile Coal

5.3.2a Swirl setting 3.0, Flame 'GC1'

The flame aerodynamics are again represented in form of streak lines in Fig.(5.5a) The three recirculation regions in the flame are similar to those obtained in the high volatile flames CV1 and CV2. The present flame GC1 is therefore also type O.

The recommended models and optimized constants for the high volatile coals (Lockwood and Rizvi (1984)) did not perform for the low volatile fuel. Substantial changes were made in the devolatilization and char burn-out modelling see sections (3.1) and (3.2) for details. For example results of predicted temperature profiles for the flame GC1 are presented for Q=2.0 (continuous line) and Q=1.2 (broken line) in Fig. (5.5b). (Q is

defined as:

$$Q = \frac{\text{The total amount of volatile matter released from the coal}}{\text{Amount of volatiles obtained from Proximate Analysis}}$$

The sensitivity of this factor to the predictions of the low volatile coal is obvious. On the other hand no sensitivity to Q was detected for the high volatile Alberta flames, see Lockwood and Rizvi (1984). Figs. (5.5c) and (5.5d) represent the profiles of volume fraction of oxygen and carbon dioxide respectively. It may be seen from the above figures that the combustion reaction close to the axis for the location nearest to the burner are under predicted. The uniform behaviour among the different fuels strongly suggests the possibility that this discrepency is due to the difficulty in approximating the real burner geometry. Since the deviations from reality are fairly minor we did not at the outset expect them to have serious consequences.

Flame GC1 is hotter than the high volatile flames CV1 and CV2 in the cooled portion of the furnace though the overall burnout is less (≈85%) than the flames CV1 and CV2 (≈100%). The reasons for the higher flame temperatures in this region are: (i) delayed combustion (ii) higher calorific value for Goodrich coal and (iii) less excess air (3% excess oxygen for flame GC1 as opposed to 8% for the flames CV1 and CV2). Figs. (5.5e) and (5.5f) give the heat flux to the cooling circuits and the incident radiation flux reacting the wall respectively. The heat fluxes for the flame GC1 is higher than the HVC flames due to the high flame temperatures.

5.3.2b. Swirl Setting 4.5, Flame 'GC2'

The results of the calculations for the flame GC2 are displayed in Figs (5.6). The aerodynamic flame structure of the flame GC2 is the same as the previous flames except for an additional but weak recirculation region at the commencement of the quarl region, see Fig. (5.6a). Again no internal recirculation zone is observed due to the high primary air flow (≈58% of the total).

Comparisons of the gas concentration profiles in terms of oxygen and carbon dioxide volume fraction are presented in Figs. (5.6c) and (5.6d) respectively. Due to the higher swirling velocity of the flame the flame GC2 is wider than flame GC1 and the burnout is higher (≈95% for flame GC2 as opposed to ≈85% for flame GC1).

Figs (5.6e) and (5.6f) represent comparisons of the heat transfer for the flame GC2.

Table (5.1)

Specifications of the coals used

Proximate Analysis (dry basis)

	Coal Valley (HVC)	Goodrich (LVC)
Volatile matter	%:34.59	24.18
Ash	%:11.10	12.61
Fixed carbon	%:54.31	63.21

Ultimate Analysis (dry basis)

c	%:68.77	77.01
H_2	%: 3.79	4.01
S	%: 0.26	0.32
N_2	%: 0.93	1.27
Ash	%:11.10	12.61
O_2	%:15.15	4.78
Heating Value (MJ/kg)	26.7	30.67

Table (5.2)

Specifications of Basic Operating Conditions of the Flames Predicted

	Coal Valley (HVC)		Goodrich (LVC)	
	CV1	CV2	GC1	GC2
Swirl setting	3.0	4.5	3.0	4.5
Fuel flow rate (kg/hr)	59.7	61.2	60.0	59.8
Primary air flow rate (kg/hr)	461.43	491.15	503.8	13.41
Secondary air flow rate (kg/hr)	342.06	320.54	180.72	295.1
Excess Oxygen (% nominal)	8.0	8.0	3.0	3.0
Primary air temperature (^{o}C)	98.0	88.0	93.0	86.0
Secondary air temperature (^{o}C)	138.0	135.0	122.0	140.0
Wall Temperature (cooling zone)	137.0	137.0	137.0	137.0
Wall emissivity	0.7	0.7	0.6	0.6
Combustibles in ash (% by wt)	0.97	0.5	50.4	28.2

Key:

CV1 = High volatile Coal Valley, Flame with swirl setting=3.0, CCRL experiment date: May 5, 1985.

CV2 = High Volatile Coal Valley flame with swirl setting = 4.5, CCRL experiment date: May 21, 1985.

GC1 = low Volatile Goodrich flame with swirl setting = 3.0, CCRL experiment date: May 23, 1985.

GC2 = Low Volatile Goodrich flame with swirl setting = 4.5, CCRL experiment date: May 27, 1985

Table (5.3)

PARTICLE SIZE RANGES FOR THE FLAMES

Coal Valley				Goodrich			
CV1		CV2		GC1		GC2	
Particle size Ranges (μm)	%	Particle size Ranges (μm)	%	Particle size Ranges (μm)	%	Particle size Ranges (μm)	%
40	18.0	40	18.0	40	11.0	40	16.0
60	66.0	60	69.0	60	63.0	60	74.0
87.5	12.0	87.5	11.0	87.5	16.0	87.5	7.0
125	4.0	125	2.0	125	10.0	125	3.0

Fig. (5.1) Furnace Geometry and Computational Grid.

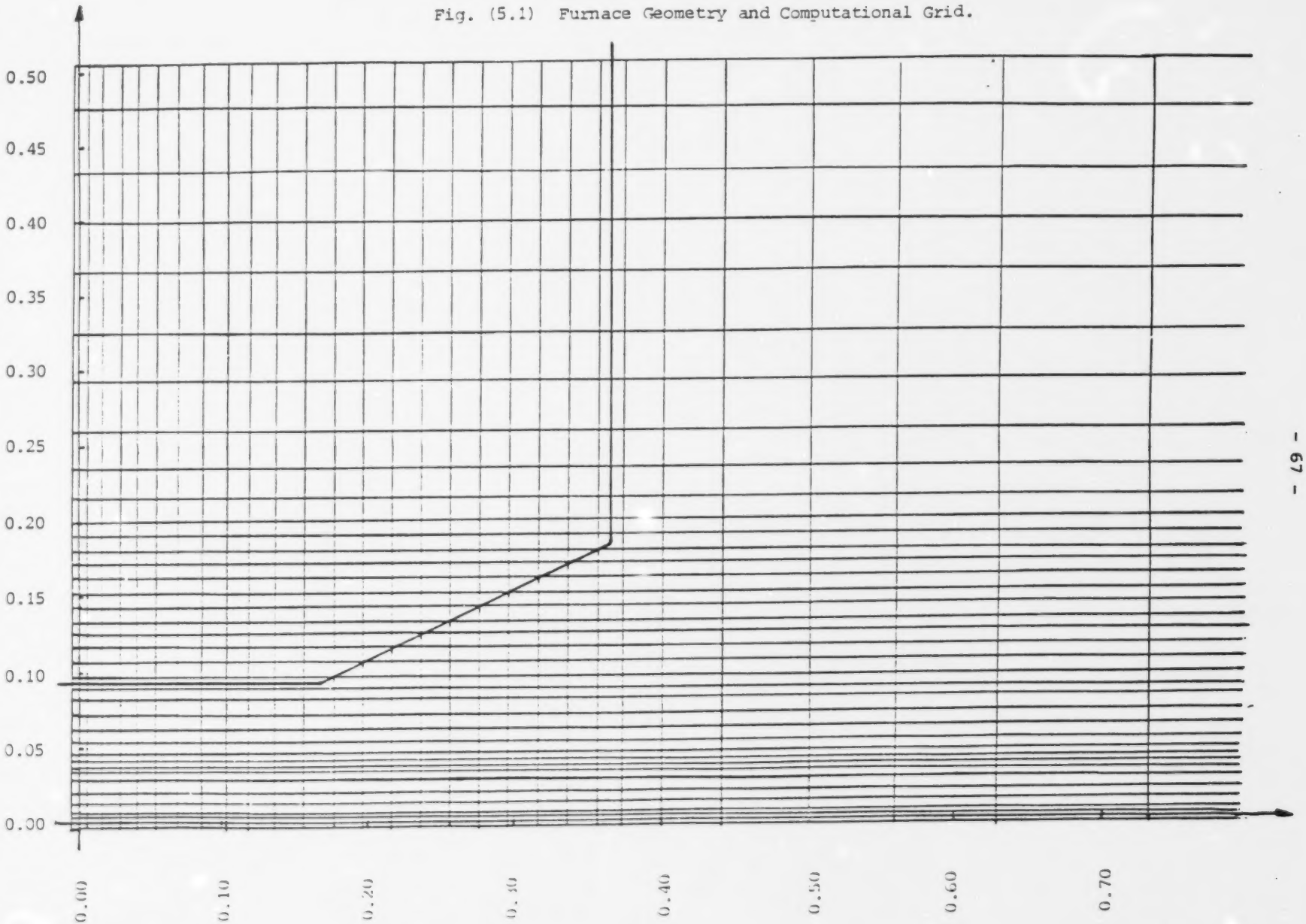

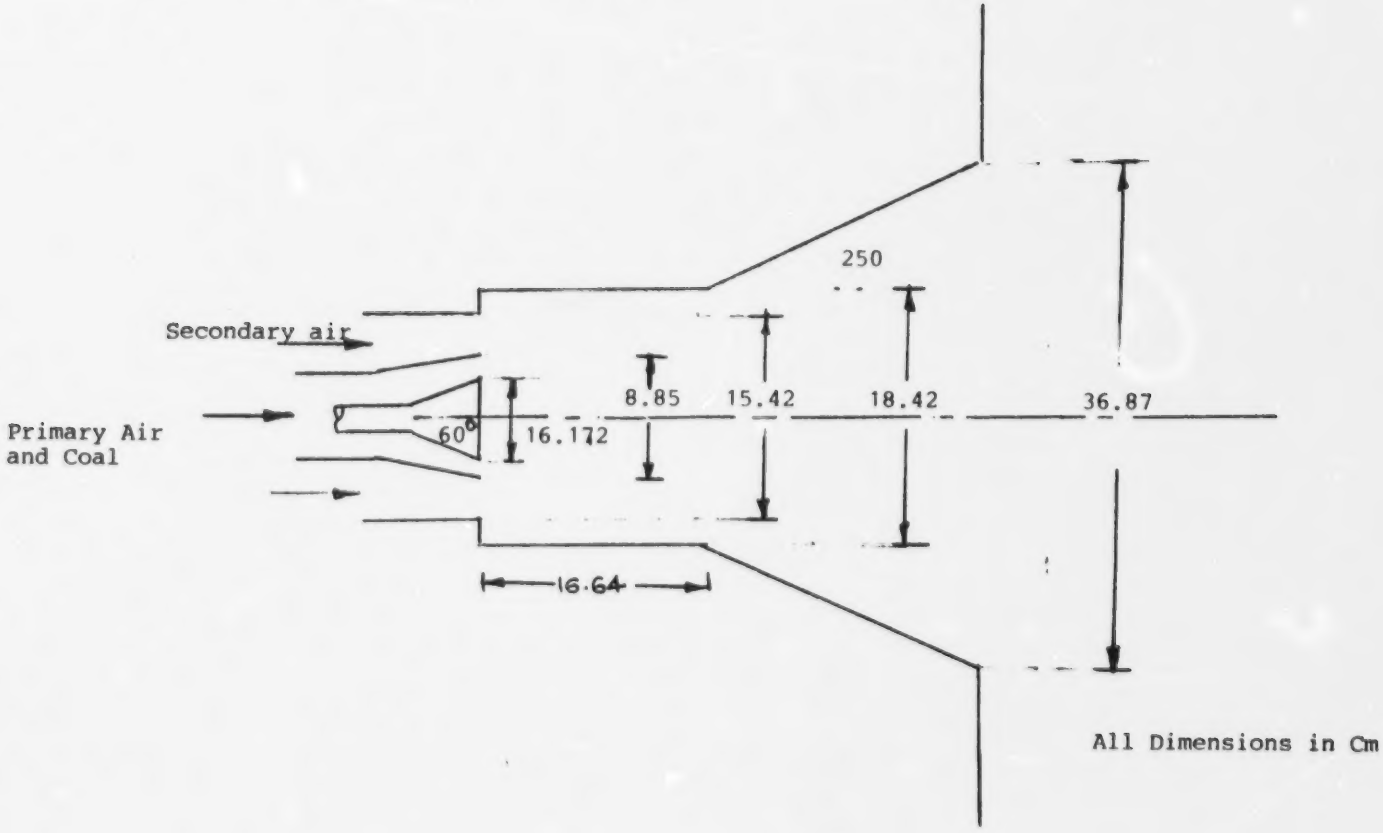

Fig. (5.2) CCRL Burner Geometry

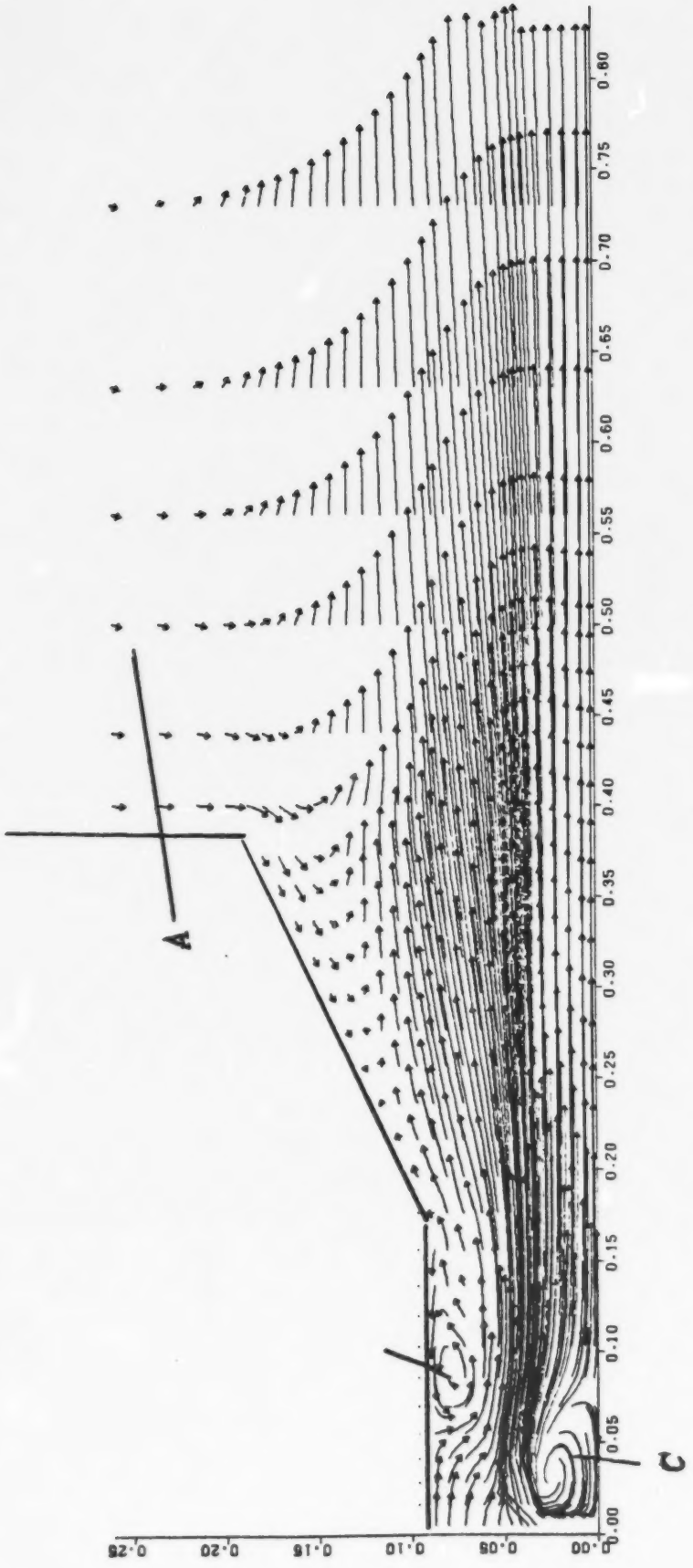
A
C
0.00
0.05
0.10
0.15
0.20
0.25
0.30
0.35
0.40
0.45
0.50
0.55
0.60
0.65
0.70
0.75
0.80
0.00
0.05
0.10
0.15
0.20
0.25

Fig. (5.3a)

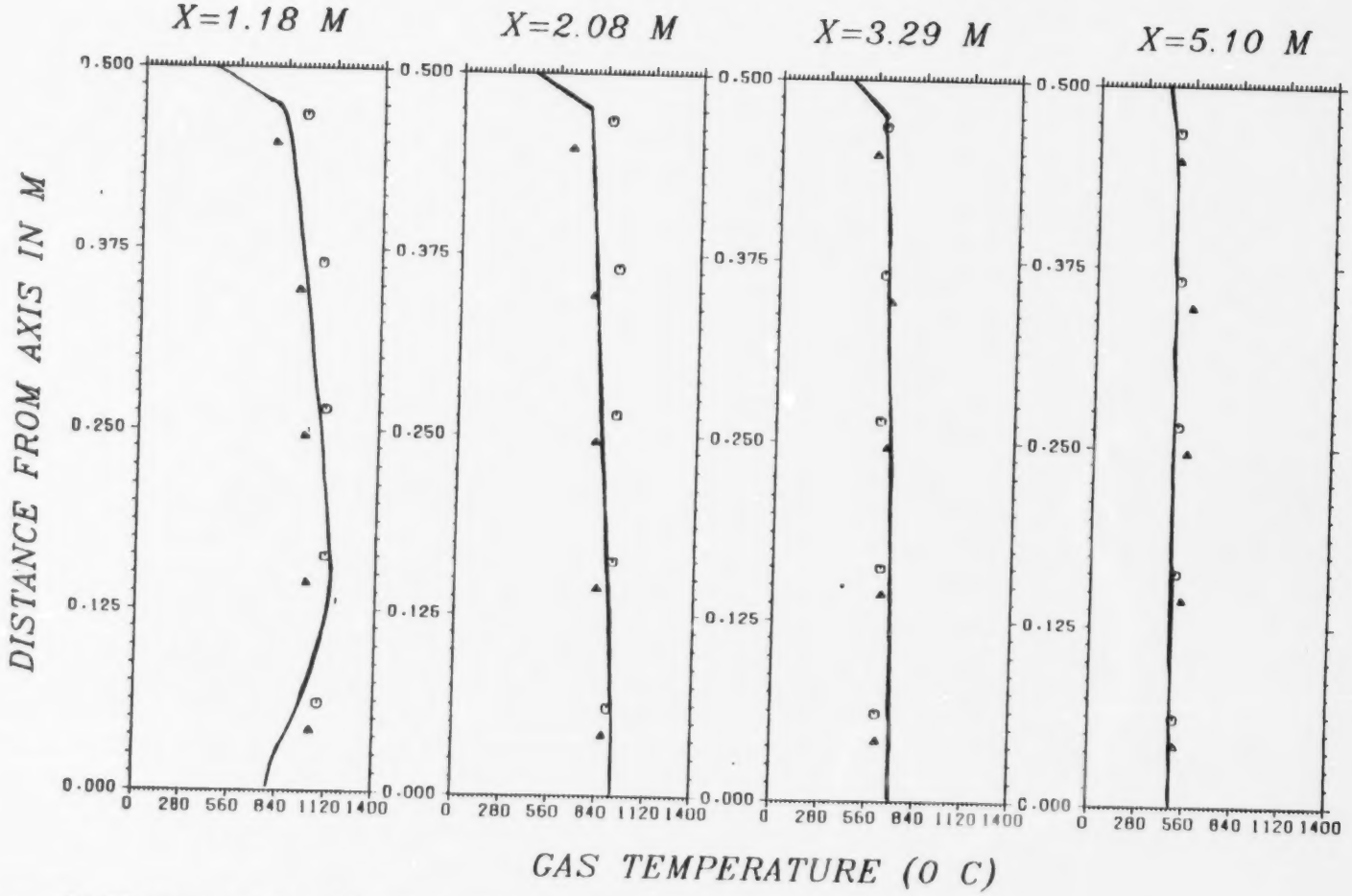
X=1.18 M
X=2.08 M
X=3.29 M
X=5.10 M
DISTANCE FROM AXIS IN M
0.500
0.375
0.250
0.125
0.000
0 280 560 840 1120 1400
GAS TEMPERATURE (0 C)
CANMET DATA ABOVE THE AXIS
CANMET DATA BELOW THE AXIS

Fig. (5.3b)

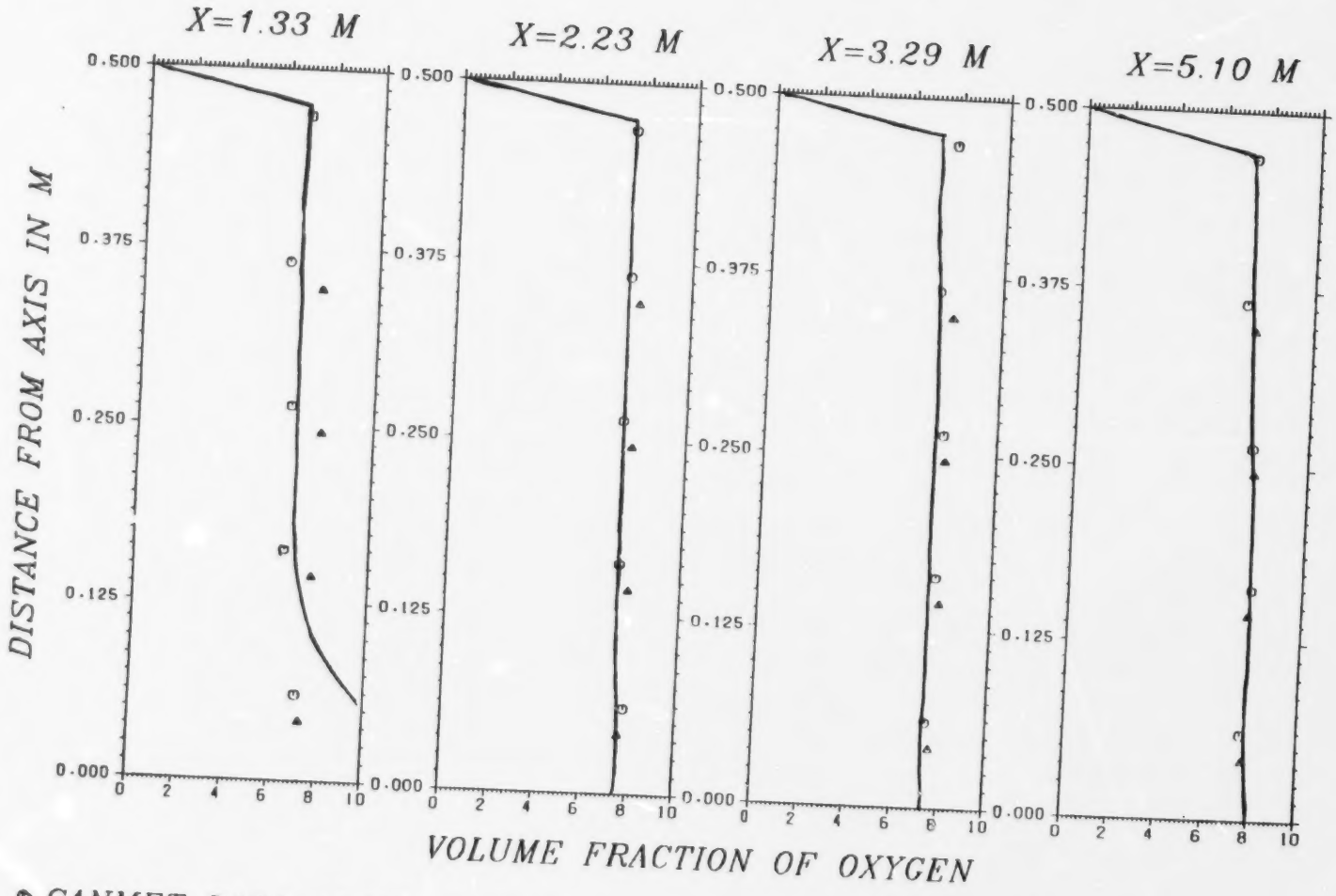
X=1.33 M
X=2.23 M
X=3.29 M
X=5.10 M
DISTANCE FROM AXIS IN M
0.500
0.375
0.250
0.125
0.000
0
2
4
6
8
10
VOLUME FRACTION OF OXYGEN
CANMET DATA ABOVE THE AXIS
CANMET DATA BELOW THE AXIS

Fig. (5.3c)

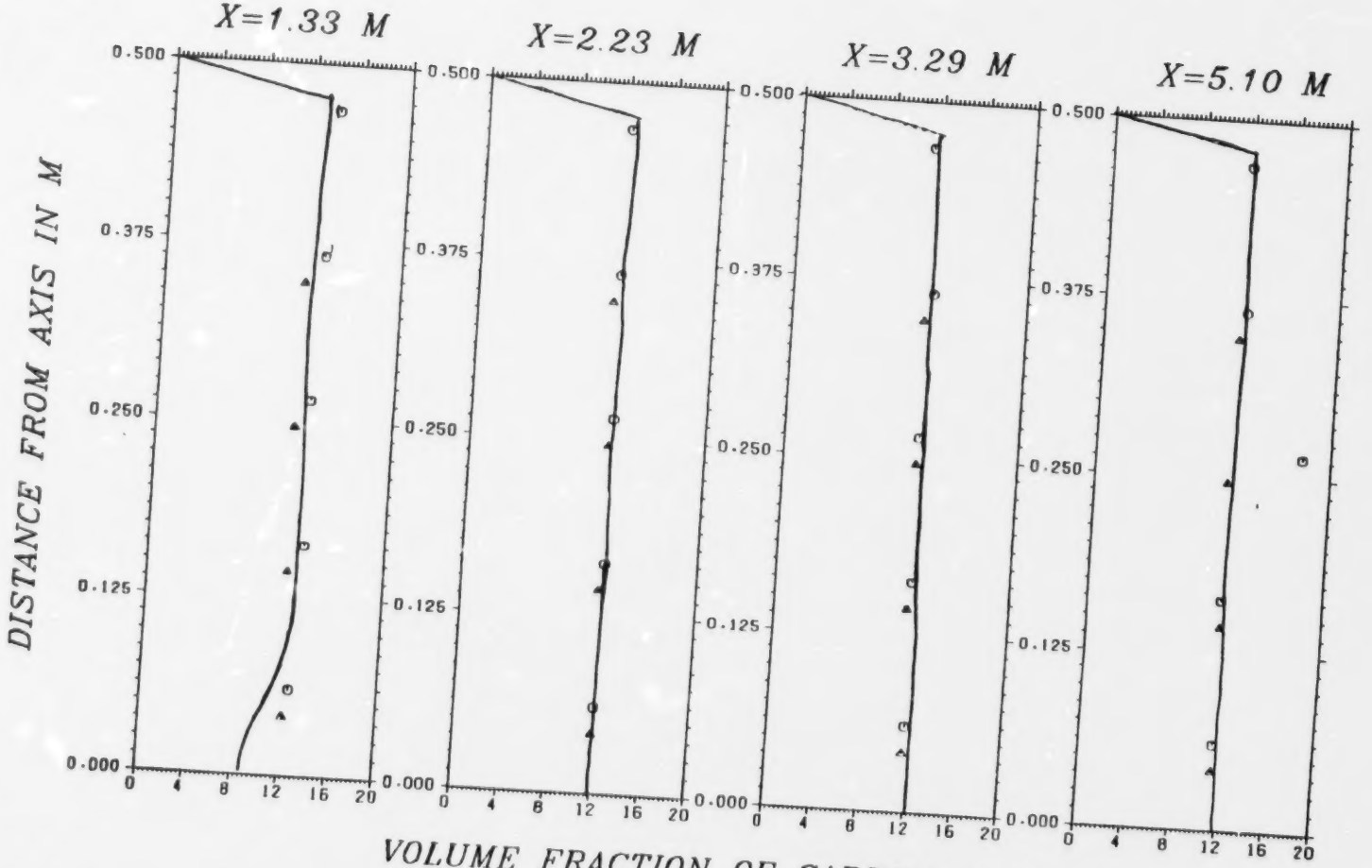
X=1.33 M
X=2.23 M
X=3.29 M
X=5.10 M
DISTANCE FROM AXIS IN M
0.500
0.375
0.250
0.125
0.000
0
4
8
12
16
20
VOLUME FRACTION OF CARBON DIOXIDE
CANMET DATA ABOVE THE AXIS
CANMET DATA BELOW THE AXIS

Fig. (5.3d)

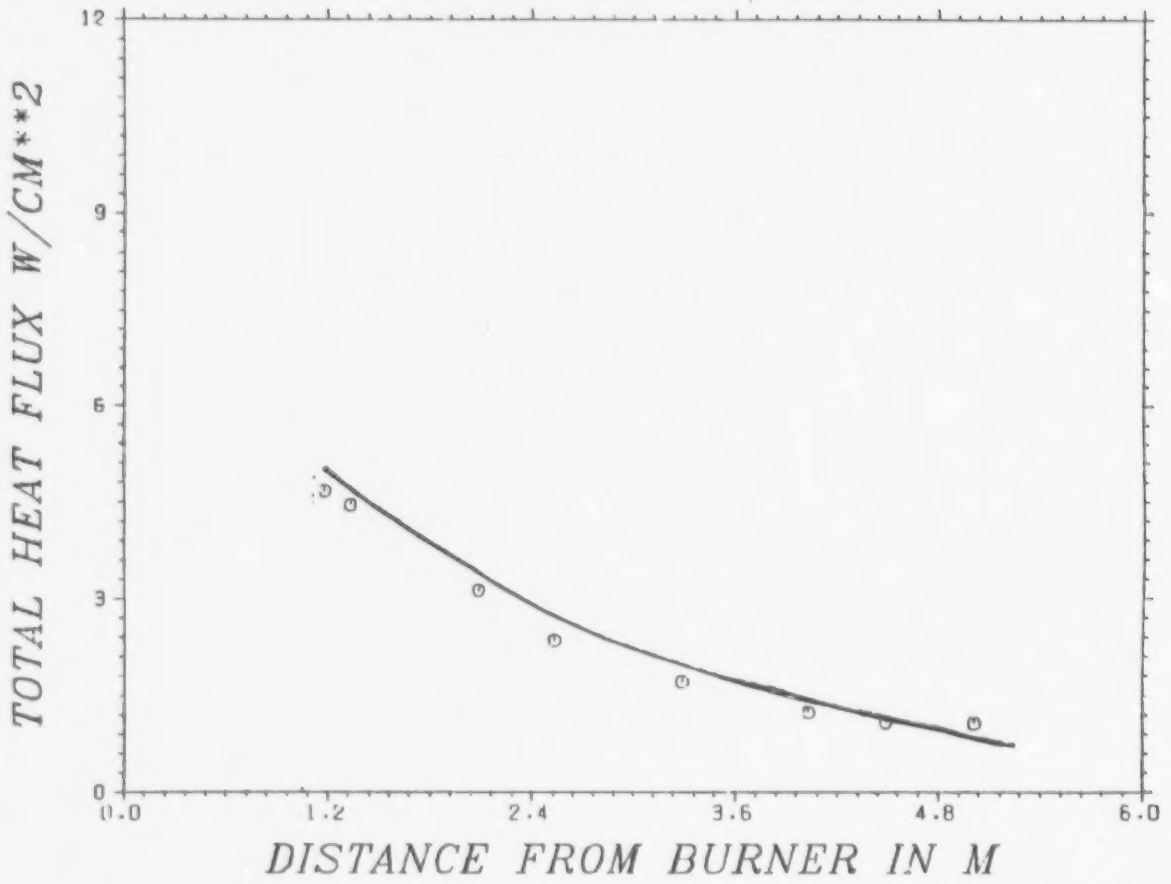
COAL VALLEY, SWIRL SETTING=3.0
TOTAL HEAT FLUX W/CM**2
12
9
6
3
0
0.0
1.2
2.4
3.6
4.8
6.0
DISTANCE FROM BURNER IN M

Fig. (5.3e)

COAL VALLEY, SWIRL SETTING=3.0

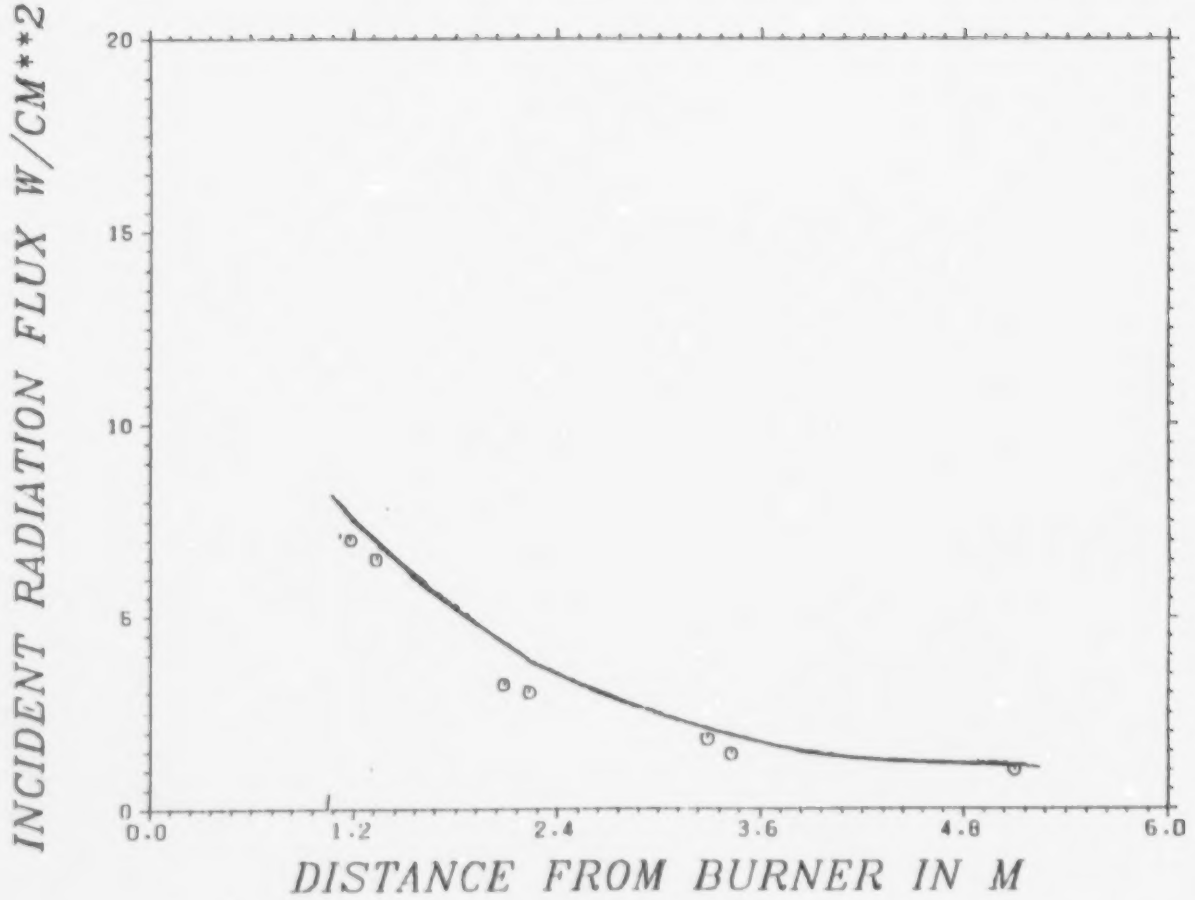

Fig. (5.3f)

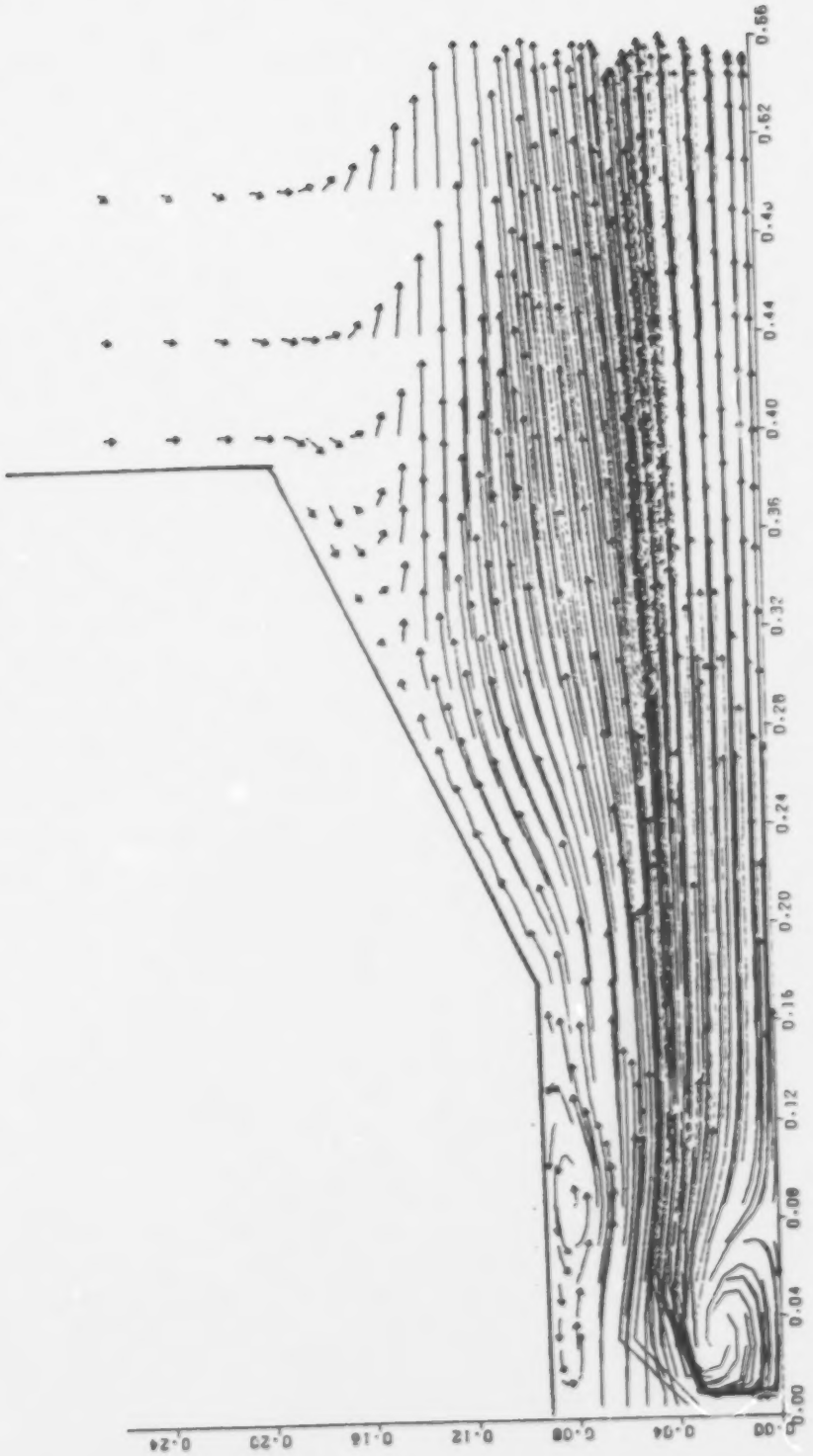
0.66
0.62
0.44
0.40
0.36
0.32
0.28
0.24
0.20
0.16
0.12
0.08
0.04
0.00
0.00
0.04
0.08
0.12
0.16
0.20
0.24

Fig. (5.4a)

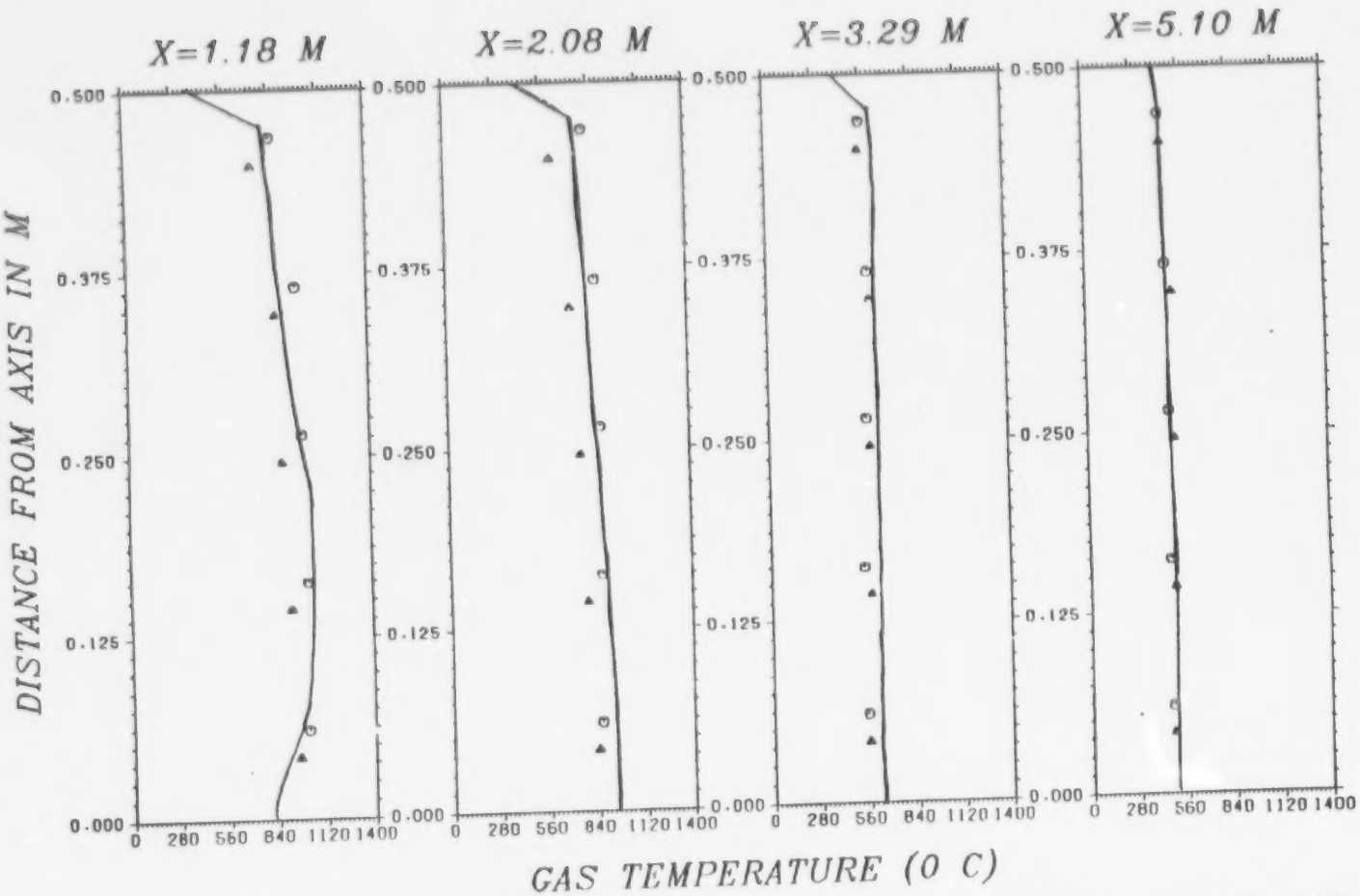
X=1.18 M
X=2.08 M
X=3.29 M
X=5.10 M
DISTANCE FROM AXIS IN M
0.500
0.375
0.250
0.125
0.000
0 280 560 840 1120 1400
GAS TEMPERATURE (0 C)
CANMET DATA ABOVE THE AXIS
CANMET DATA BELOW THE AXIS

Fig. (5.4b)

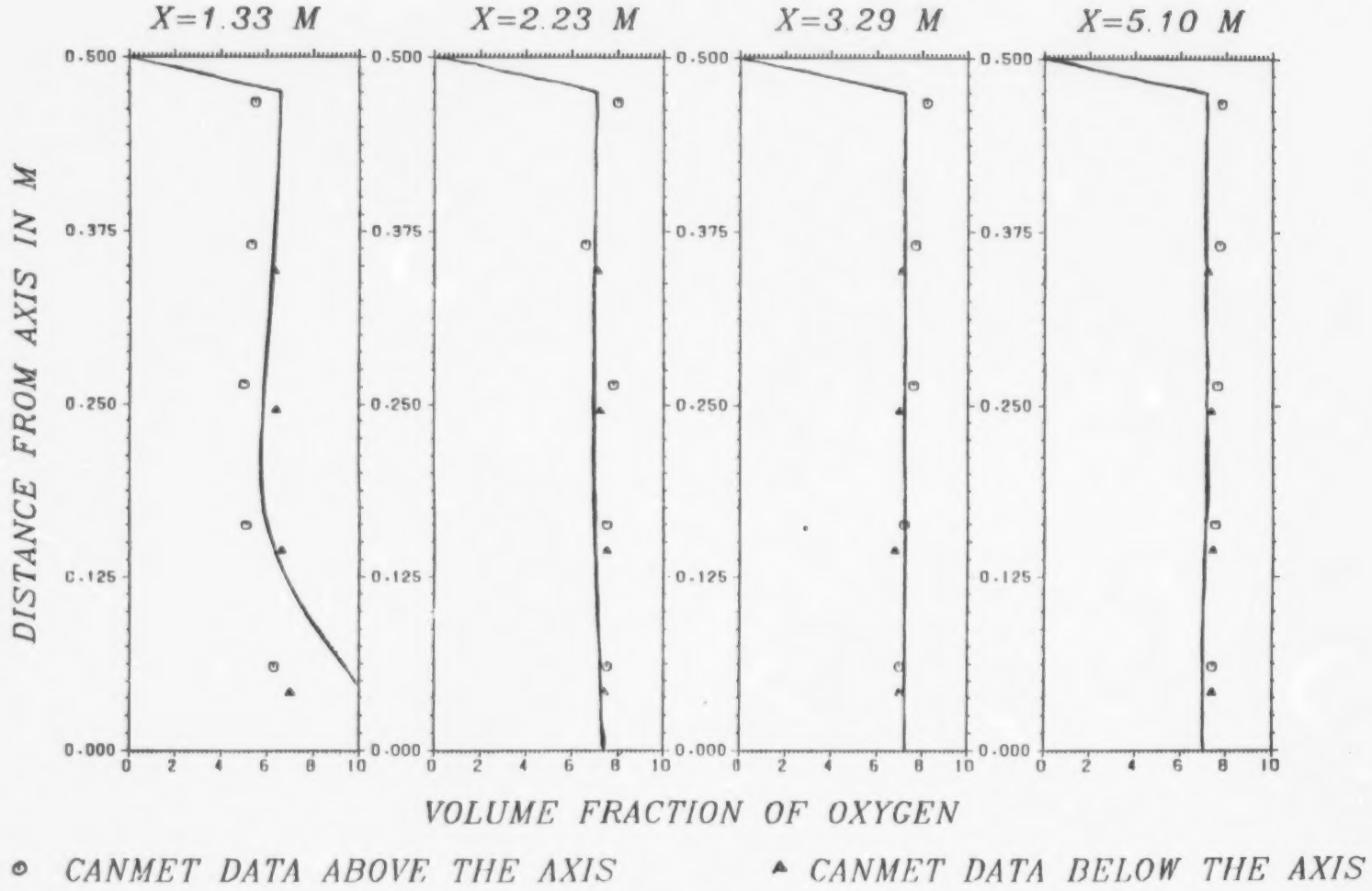
X=1.33 M
X=2.23 M
X=3.29 M
X=5.10 M
DISTANCE FROM AXIS IN M
0.500
0.375
0.250
0.125
0.000
0
2
4
6
8
10
VOLUME FRACTION OF OXYGEN
CANMET DATA ABOVE THE AXIS
CANMET DATA BELOW THE AXIS

Fig (5.4c)

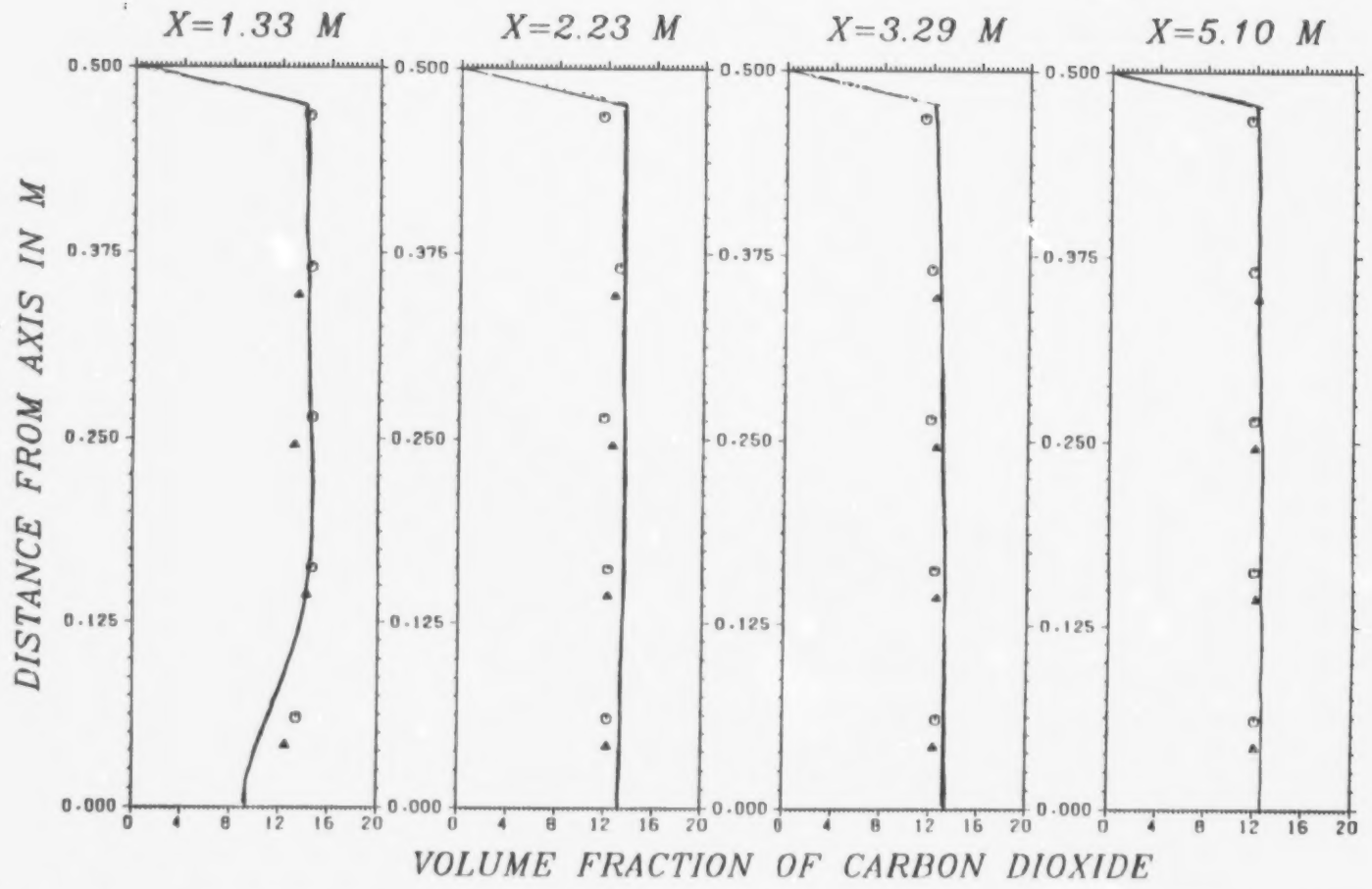
X=1.33 M
X=2.23 M
X=3.29 M
X=5.10 M
DISTANCE FROM AXIS IN M
0.500
0.375
0.250
0.125
0.000
0
4
8
12
16
20
VOLUME FRACTION OF CARBON DIOXIDE
CANMET DATA ABOVE THE AXIS
CANMET DATA BELOW THE AXIS

Fig. (5.4d)

COAL VALLEY, SWIRL SETTING=4.5

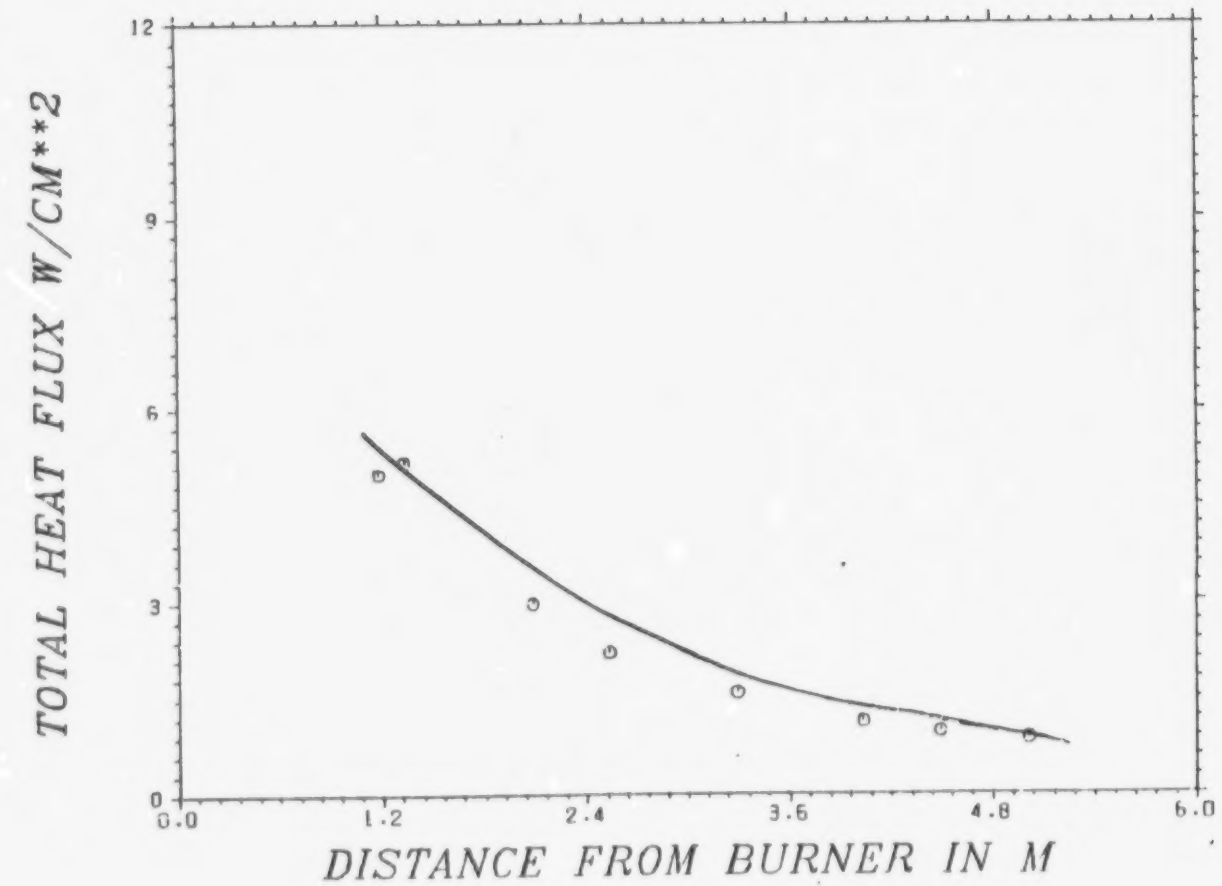

Fig.(5.4e)

COAL VALLEY, SWIRL SETTING=4.5

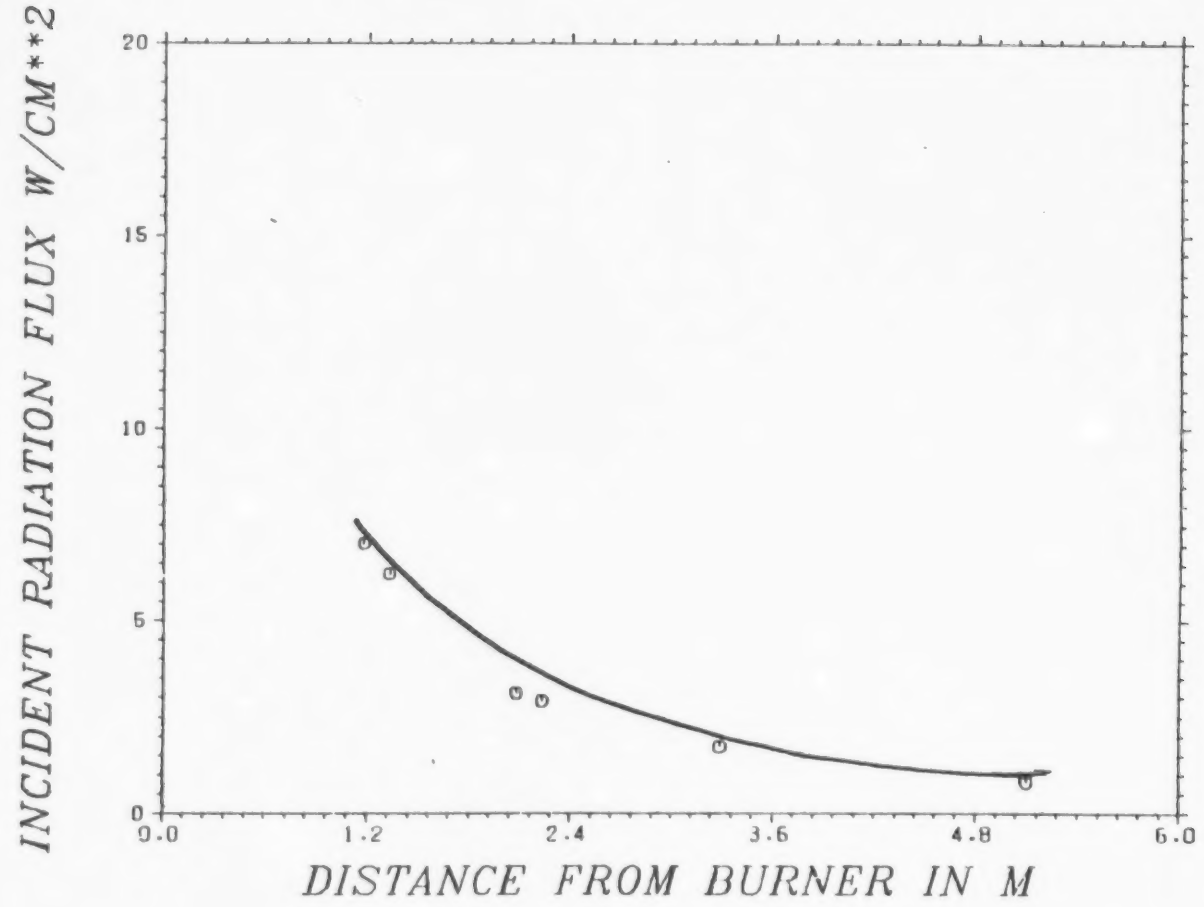

Fig. (5.4f)

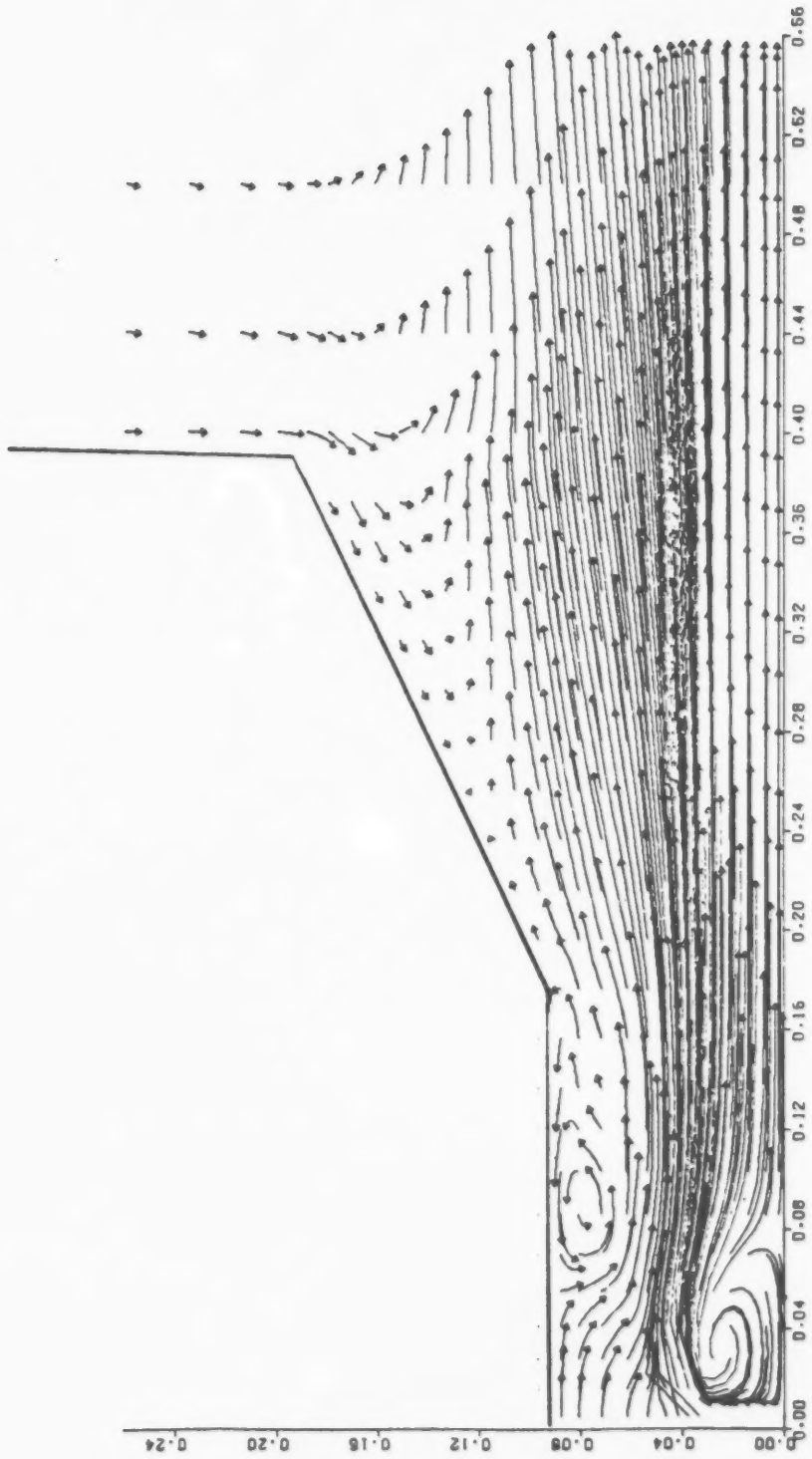
0.00
0.04
0.08
0.12
0.16
0.20
0.24
0.28
0.32
0.36
0.40
0.44
0.48
0.52
0.56
0.00
0.04
0.08
0.12
0.16
0.20
0.24

Fig. (5.5a)

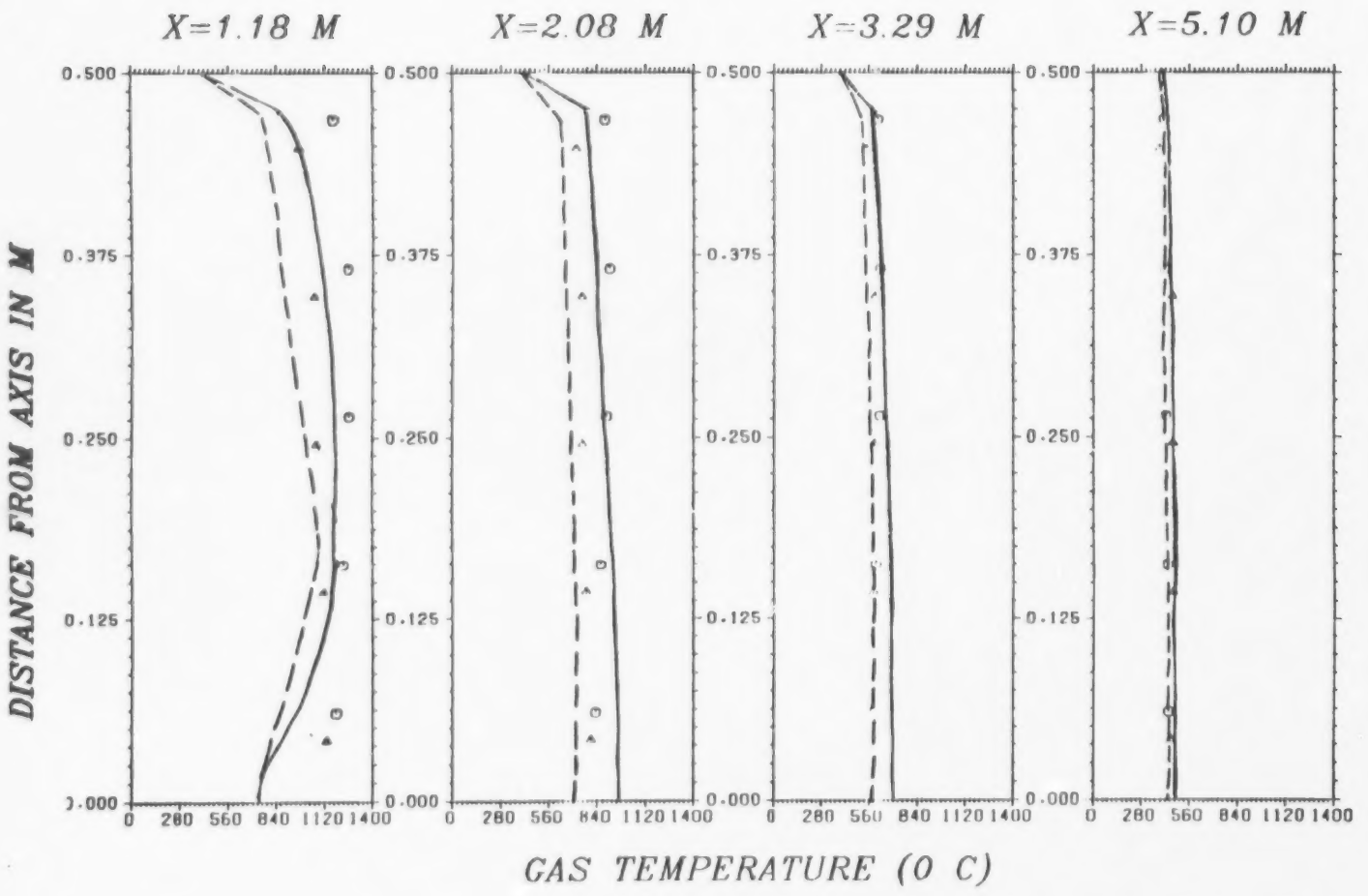
X=1.18 M
X=2.08 M
X=3.29 M
X=5.10 M
DISTANCE FROM AXIS IN M
0.500
0.375
0.250
0.125
0.000
0 280 560 840 1120 1400
GAS TEMPERATURE (0 C)
CANMET DATA ABOVE THE AXIS
CANMET DATA BELOW THE AXIS

Fig. (5.5b)

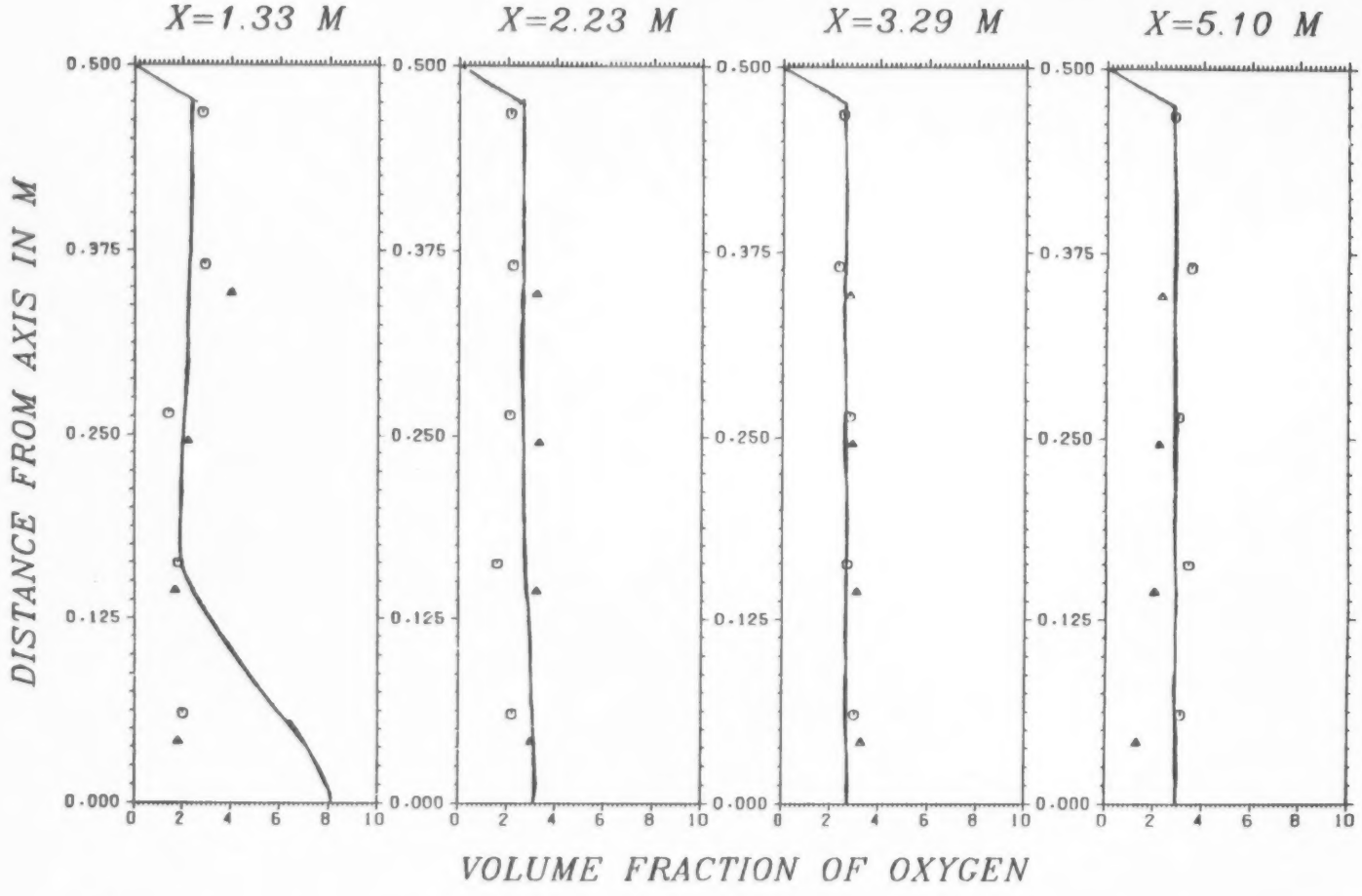
X=1.33 M
X=2.23 M
X=3.29 M
X=5.10 M
DISTANCE FROM AXIS IN M
0.500
0.375
0.250
0.125
0.000
0
2
4
6
8
10
VOLUME FRACTION OF OXYGEN
CANMET DATA ABOVE THE AXIS
CANMET DATA BELOW THE AXIS

Fig. (5.5c)

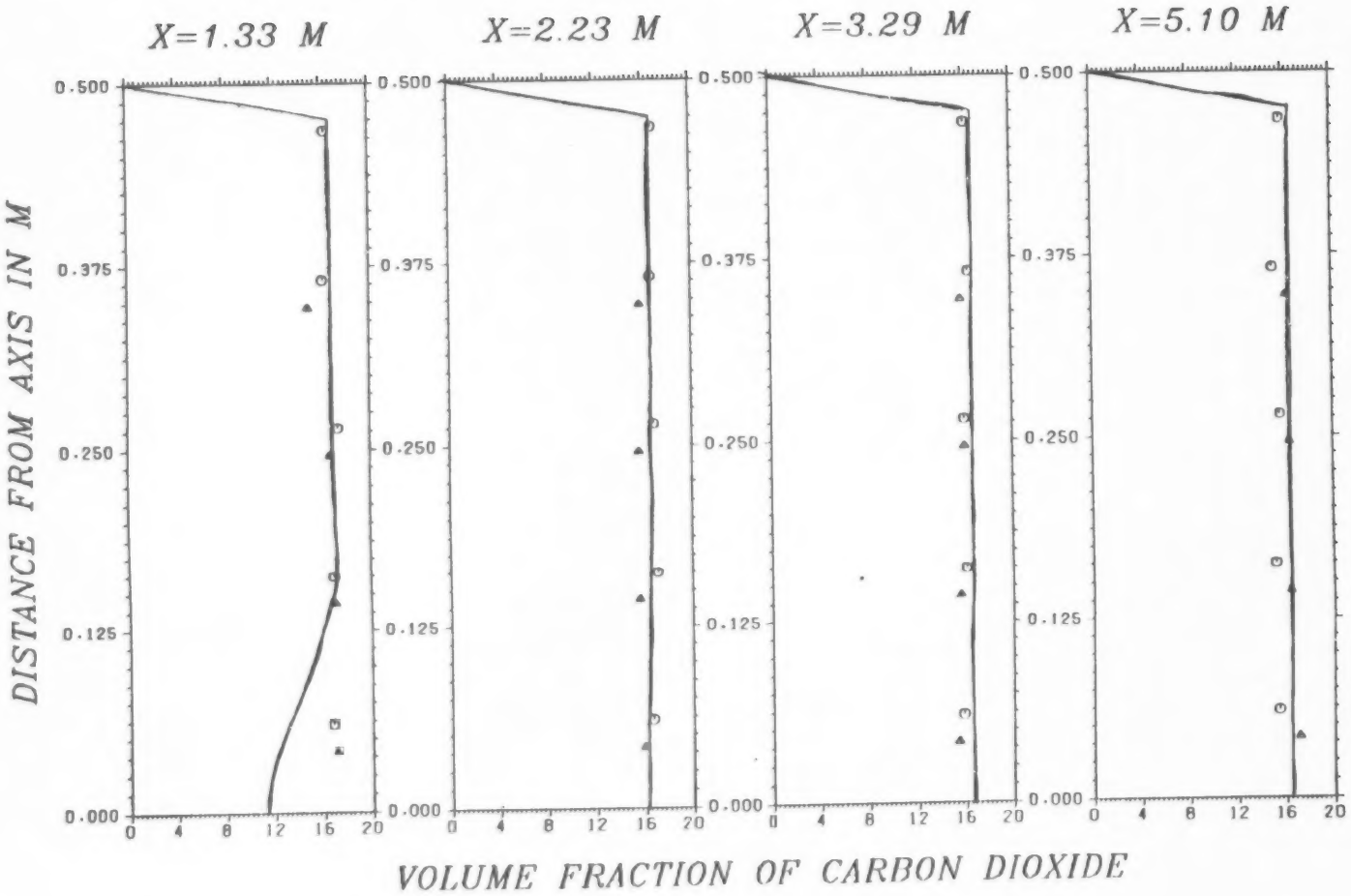
X=1.33 M
X=2.23 M
X=3.29 M
X=5.10 M
DISTANCE FROM AXIS IN M
0.500
0.375
0.250
0.125
0.000
0
4
8
12
16
20
VOLUME FRACTION OF CARBON DIOXIDE
CANMET DATA ABOVE THE AXIS
CANMET DATA BELOW THE AXIS

Fig. (5.5d)

GOODRICH COAL, SWIRL SETTING=3.0

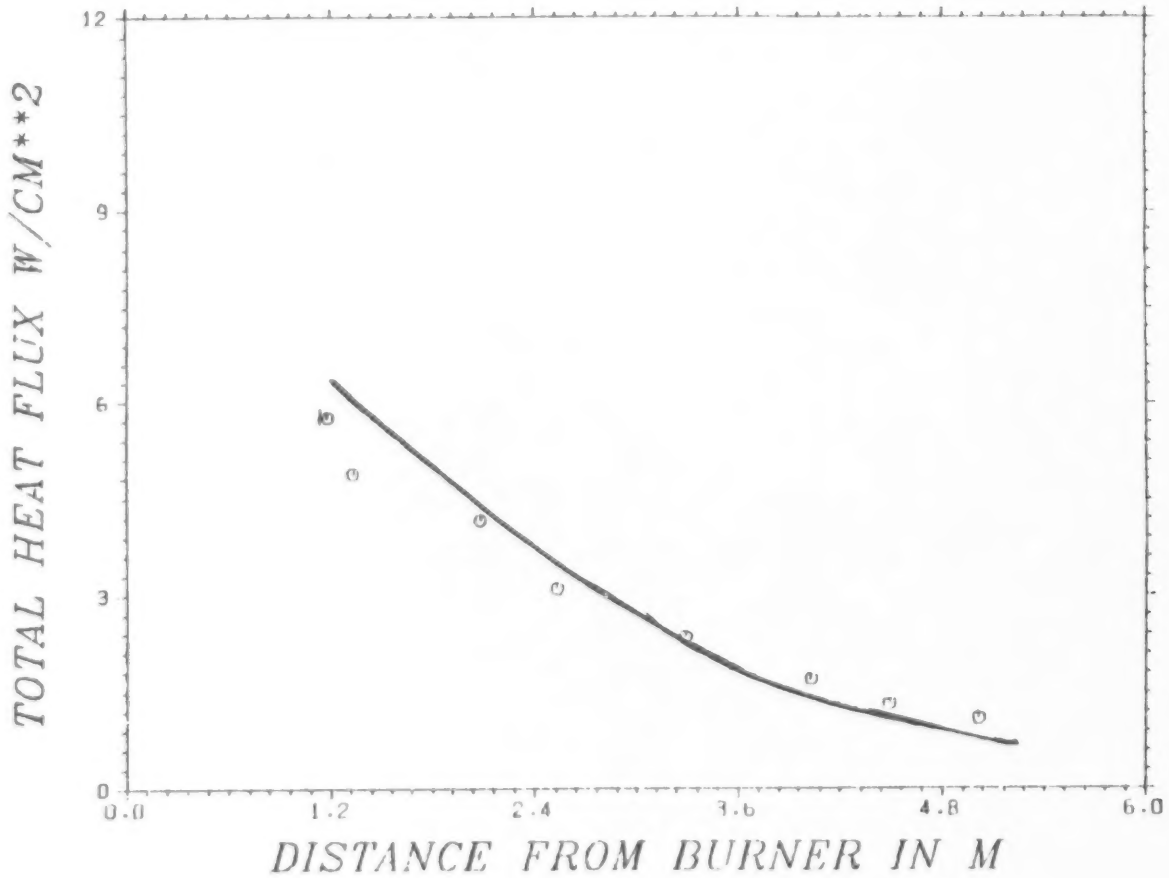

Fig. (5.5e)

GOODRICH COAL, SWIRL SETTING=3.0

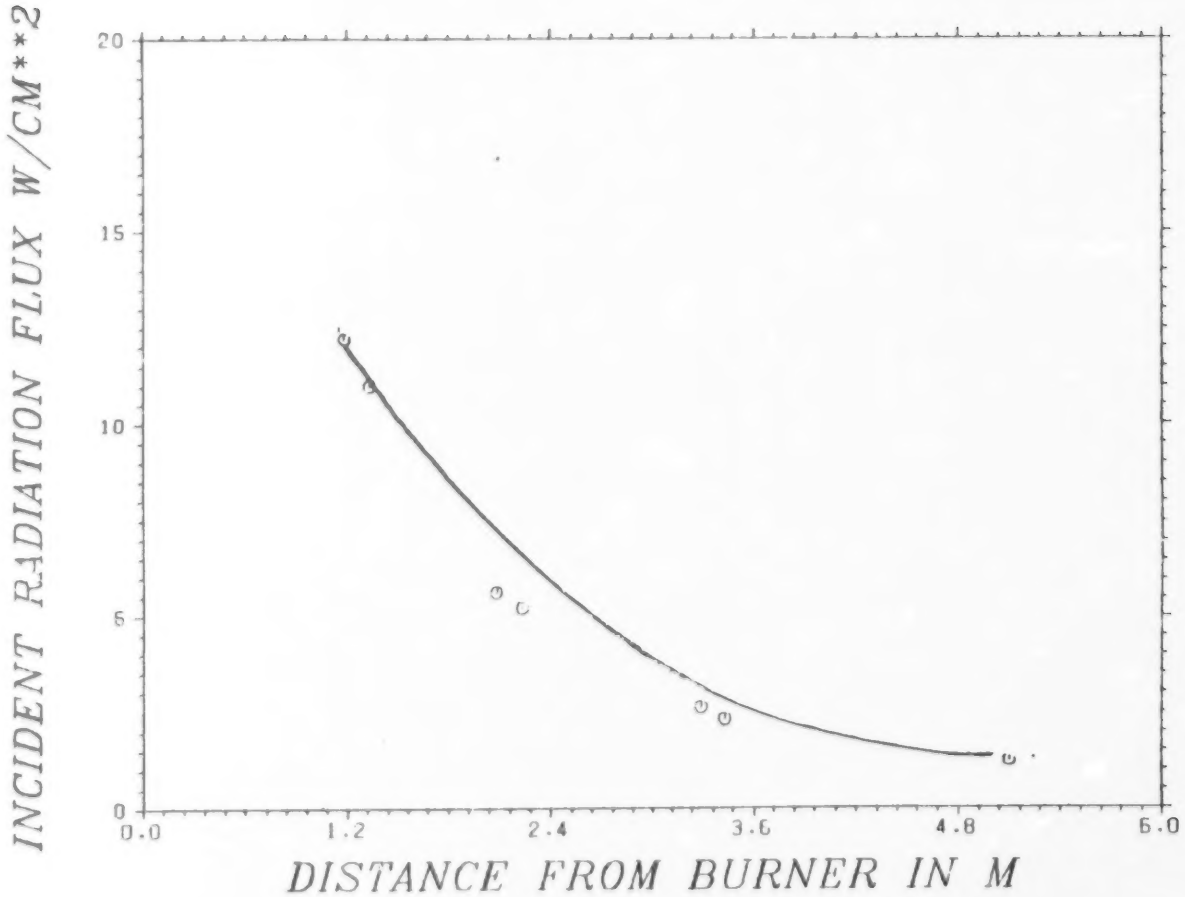

Fig. (5.5f)

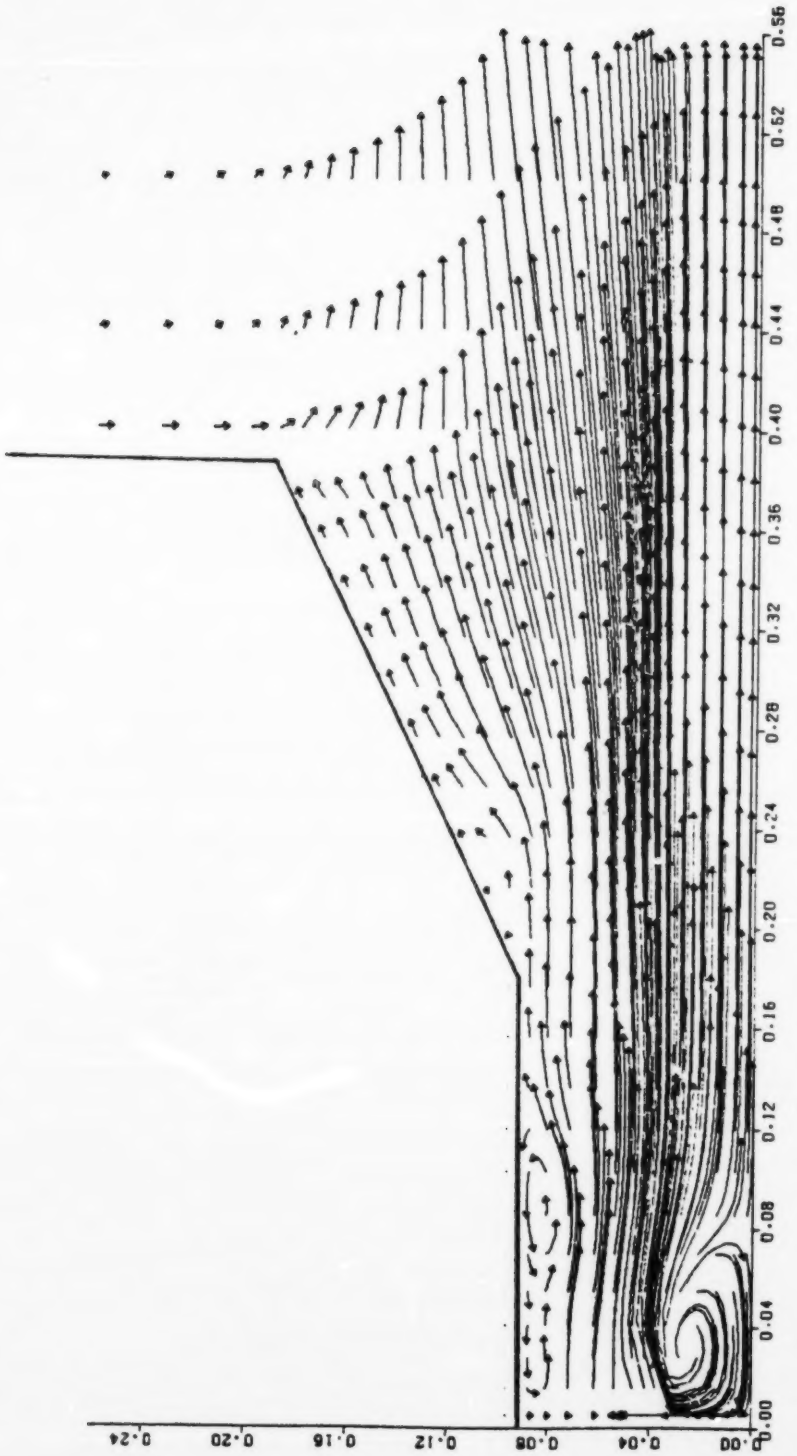
0.00
0.04
0.08
0.12
0.16
0.20
0.24
0.28
0.32
0.36
0.40
0.44
0.48
0.52
0.56
0.00
0.04
0.08
0.12
0.16
0.20
0.24

Fig. (5.6a)

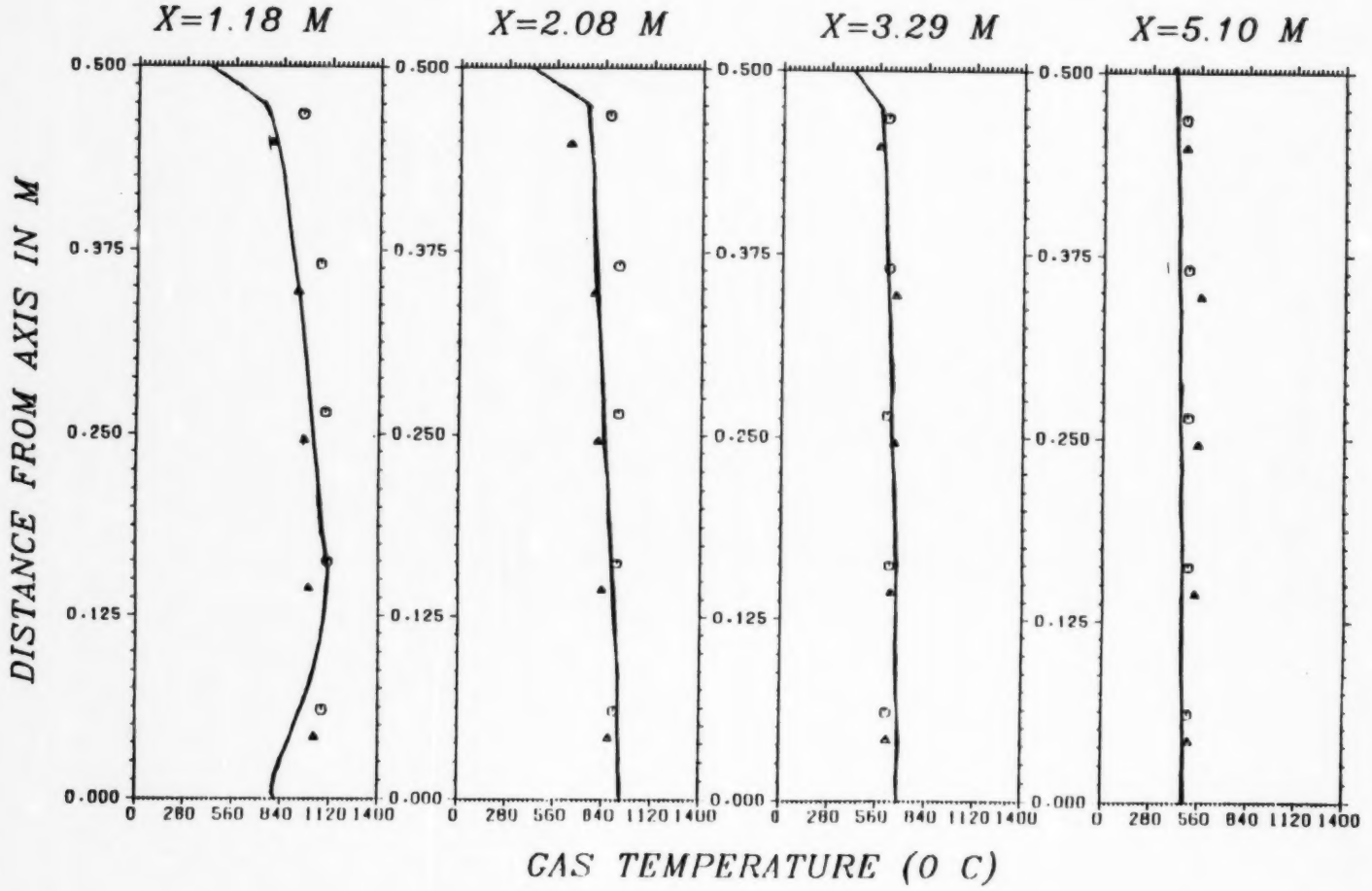
X=1.18 M
X=2.08 M
X=3.29 M
X=5.10 M
DISTANCE FROM AXIS IN M
0.500
0.375
0.250
0.125
0.000
0 280 560 840 1120 1400
GAS TEMPERATURE (0 C)
CANMET DATA ABOVE THE AXIS
CANMET DATA BELOW THE AXIS

Fig. (5.6b)

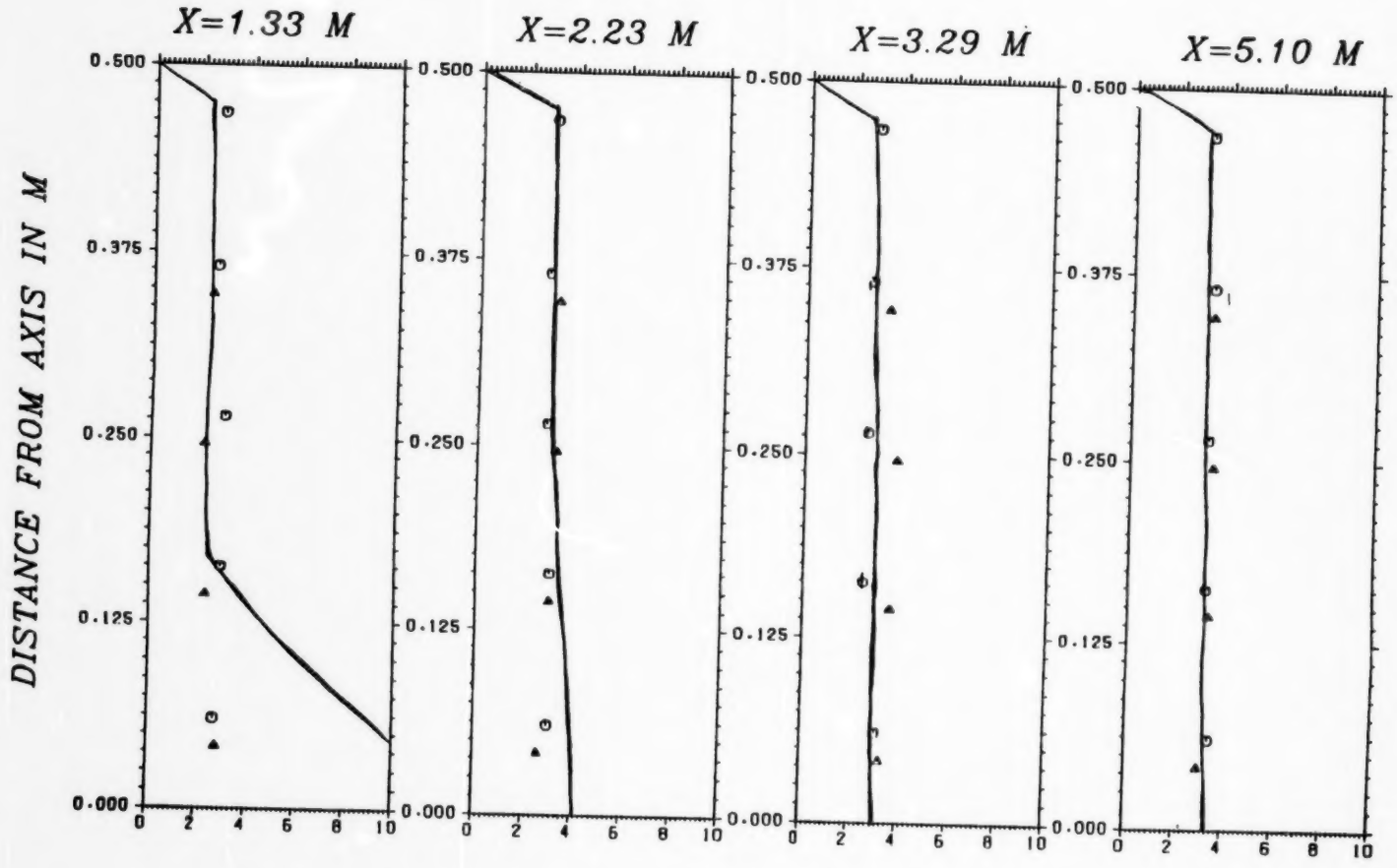
X=1.33 M
X=2.23 M
X=3.29 M
X=5.10 M
DISTANCE FROM AXIS IN M
0.500
0.375
0.250
0.125
0.000
0 2 4 6 8 10
VOLUME FRACTION OF OXYGEN
CANMET DATA ABOVE THE AXIS
CANMET DATA BELOW THE AXIS

Fig. (5.6c)

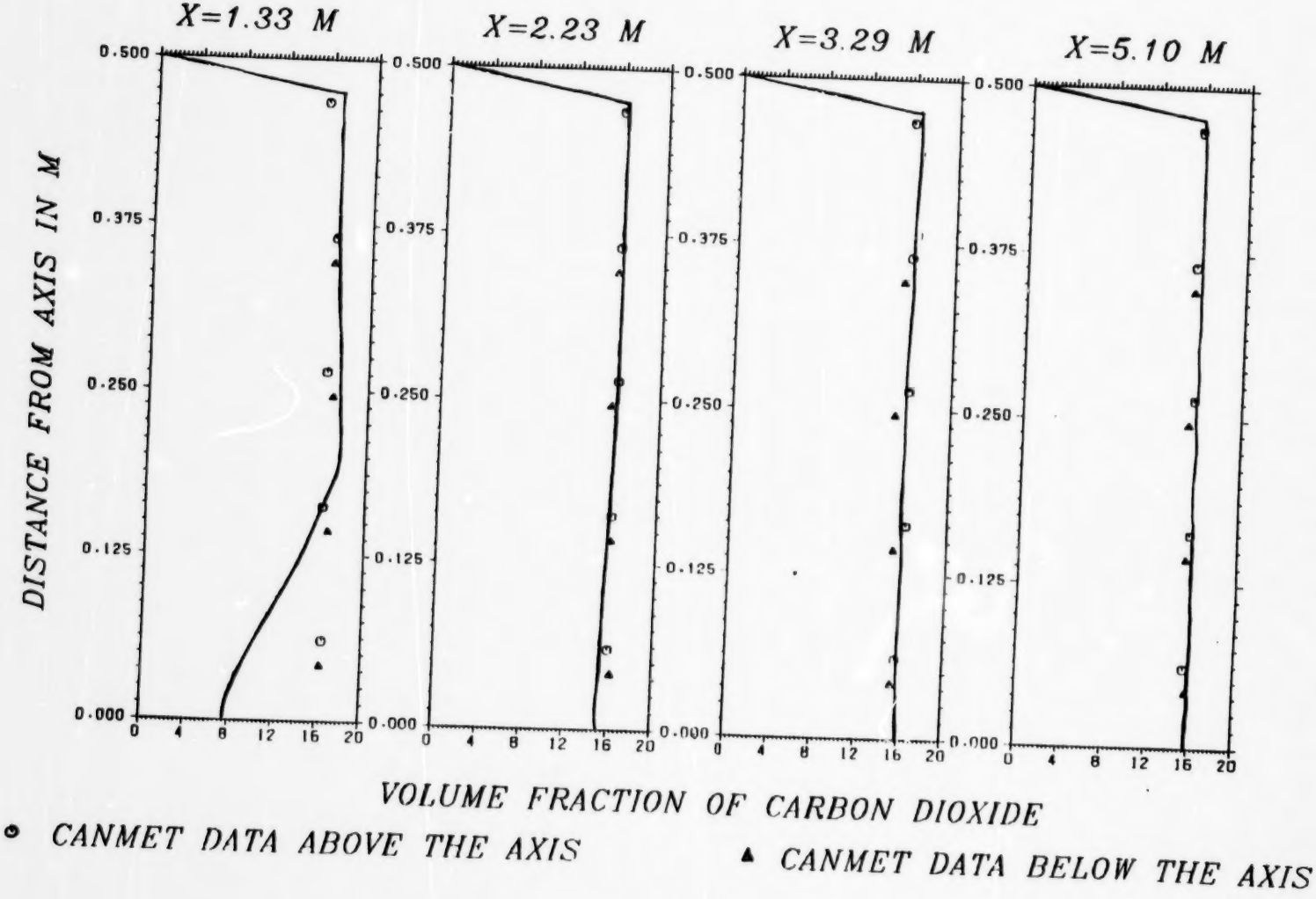
X=1.33 M
X=2.23 M
X=3.29 M
X=5.10 M
DISTANCE FROM AXIS IN M
0.500
0.375
0.250
0.125
0.000
0 4 8 12 16 20
VOLUME FRACTION OF CARBON DIOXIDE
CANMET DATA ABOVE THE AXIS
CANMET DATA BELOW THE AXIS

Fig. (5.6d)

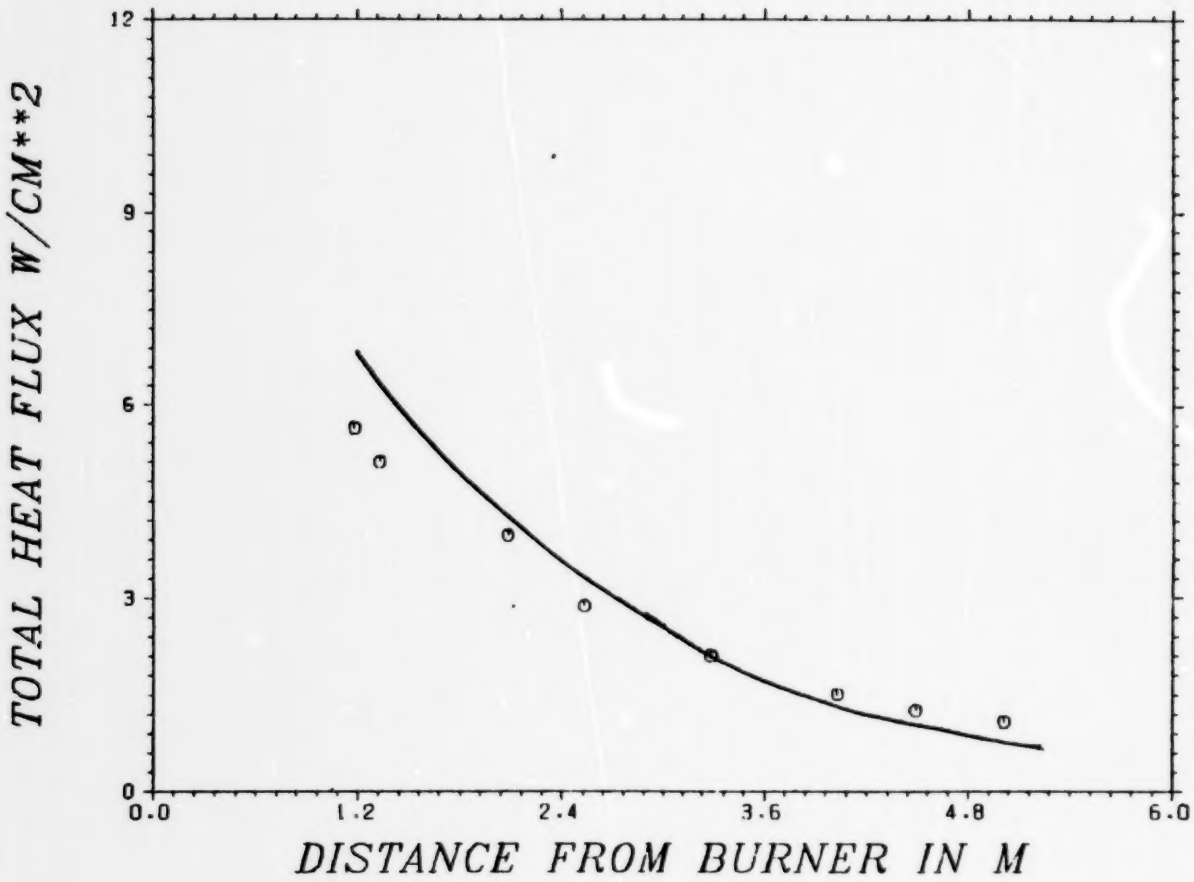
GOODRICH COAL, SWIRL SETTING=4.5
TOTAL HEAT FLUX W/CM**2
12
9
6
3
0
0.0
1.2
2.4
3.6
4.8
6.0
DISTANCE FROM BURNER IN M

Fig.(5.6e)

GOODRICH COAL, SWIRL SETTING=4.5

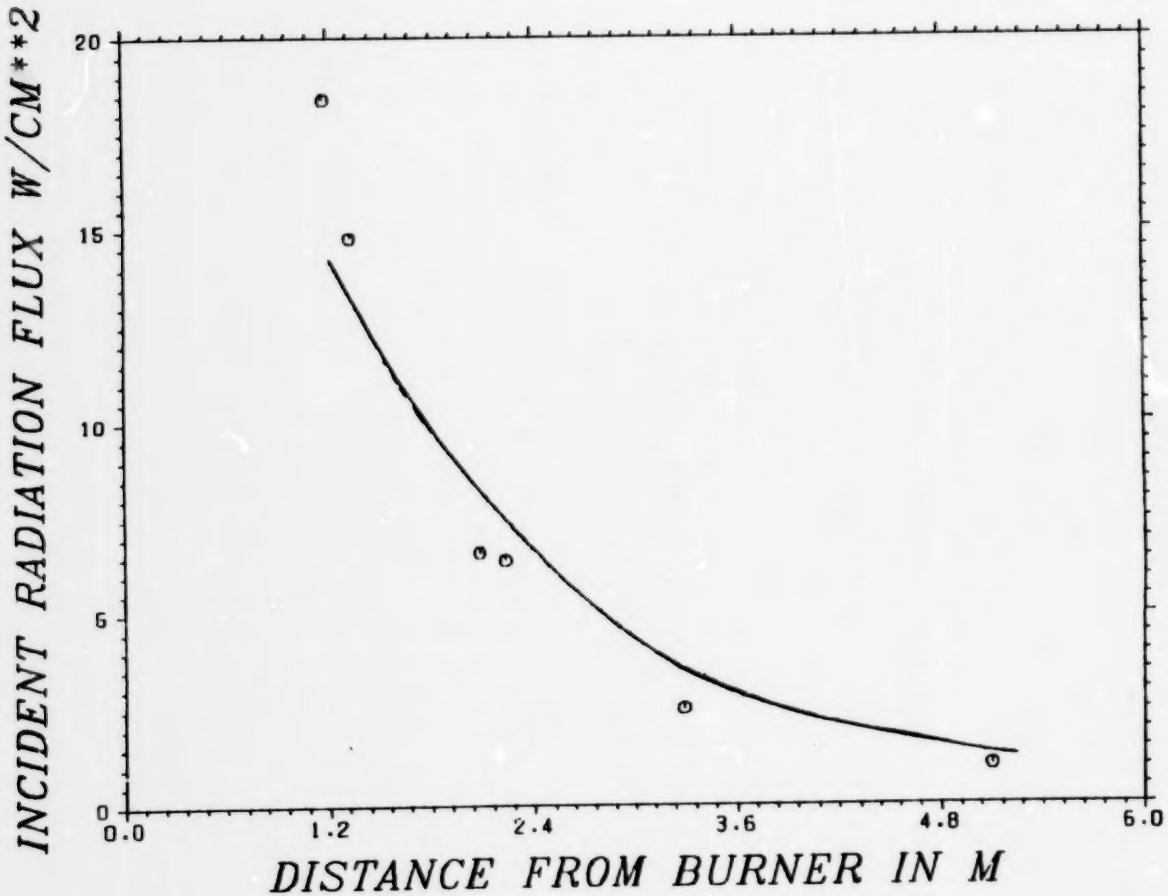

Fig. (5.6f)

6. Concluding Remarks

The following conclusions are drawn on the basis of the present predictive study:

(i) In general the results of the predictions for the high volatile flames CV1 and CV2 and for the low volatile flames GC1 and GC2 appear to be quite satisfactory.

(ii) A satisfactory level of universality is observed in the recommended physical modelling and model constants for the high volatile coals.

(iii) The predictions of the two low volatile flames suggest the universality of model constants for the low volatile flames as well.

(iv) However, the modelling found suitable for the high volatile flames requires to be modified for the low volatile ones.

(v) The modelling of the devolatilization process, the amount of volatiles released as well as the char burn out model are critical for low volatile flames.

(vi) The good prediction of the low volatile flames requires a high Q factor, a modified devolatilization model and a modified char burn out kinetics relative to the recommendations for the high volatile coals.

(vii) Contrary to expectations no 'internal' recirculation zone is developed for swirl setting of 4.5 (swirl no. = 0.75) for the high as well as low volatile flames.

(viii) The chemical reaction close to the axis at the upstream end of the combustor is uniformally under predicted for all the flames predicted considered probably due to small approximations made in simulating the geometry of the burner.

REFERENCES

1/ Abbas, A.S., Koussa, S.S. and Lockwood, F.C. (1981). "The Prediction of the Particle Laden Gas Glows", 18th Symposium (Int.) on Combustion, The Combustion Institute, p. 1427".

2/ Abbas, A.S. (1982). "Predicting the Performance of Heavy Oil-Fired Combustors". PhD. Thesis, University of London.

3/ Anthony, D.B., Howard, J.B., Hottel, H.C. and Meissner, H.P. (1975). "Rapid Devolatilization of Pulverized Coal", 15th Symposium (Int.) on Combustion, The Combustion Institute, p. 1303.

4/ Baum, D.L. and Street, P.J. (1971). "Predicting the Combustion Behaviour of Coal Particles", Combustion Science and Technology, Vol. 3, pp. 231-243.

5/ Badzioch, S. and Hawkesley, P.G.W. (1970). "Kinetics of Thermal Decomposition of Pulverized Coal Particle", Ind. Eng. Chem. Process Des. Develop., Journal of the Institute of Fuel, p. 377.

6/ Benodekar, R.W., Goddard, A.J.H., Gosman, A.D., and Issa, R.I. (1983). "Numerical Prediction of Turbulent Flow Over Surface Mounted Ribs", The American Society of Mechanical Engineers, 83-FE-13.

7/ Crowe, C.T. (1974). "A Computational Model for the Gas Droplet Flow Field in the Vicinity of an Atomizer", Western States Section, the Combustion Institute, Paper No. 74-25.

8/ Caretto, L.S. Gosman, A.D., Patankar, S.V. and Spalding D.B. (1972). "Two Calculation Procedures for Steady Three-Dimensional Flows with Recirculation", Proceedings of 3rd Int. Conference on Numerical Methods in Fluid Mechanics, 60-68.

9/ Eddinger, R.T., Friedman, L.D. and Rau, E. (1966). "Devolatilization of Coal in a Transport Reactor", Fuel 45, 245-252.

10/ Essenhigh, R.H. (1961). J. Inst. of Fuel 34, 16.

11/ Essenhigh, R.H. (1981). "Fundamentals of Coal Combustion", Chapter 19. Chemistry of Coal Utilization, Second Supplementary Volume, Editor, M.A. Elliot, Wiley Interscience Publication, New York.

12/ Field, M.A. (1969). "Rate of Combustion of Size Graded Fractions of Char from a Low-Rank Coal Between 1200°K and 2000°K, Combustion and Flame, 13, p. 237.

13/ Field, M.A. (1970). "Measurements of the Effect of Rank on Combustion Rates of Pulverized Coal", Combustion and Flame, 14, 237-248.

14/ Field, M.A., Gill, D.W., Morgan, B.B. and Hawksley, P.G.W. (1967). "Combustion of Pulverized Coal", The British Coal Utilization Research Association, Leatherhead.

15/ Gibson, M.M. and Morgan, B.B., (1970). J. Inst. Fuel, 517-523.

16/ Gosman, A.D. and Ideriah, F.J.K. (1976). "TEACH-T: A General Computer Program for Two-Dimensional, Recirculating Flows', Fluids Section Report, Mech. Engg. Dept., Imperial College, London.

17/ Gibb, J. (1973). Central Electricity Board, Internal Note, MRM 85.

18/ Gibb, J. (1977). "Central Electricity Generating Board, Southampton, England, Private Communication.

19/ Gosman, A.D., Pun, W.M., Runchal, A.K., Spalding, D.B. and Wolfshtein, M. (1969). "Heat and Mass Transfer in Recirculating Flows", Academic Press, London and New York.

20/ Hughes, P. (1985). "Experimental data H on High/Low Volatile Coals". CCRL Furnace CANMET, Canada, Private Communication.

21/ Hamor, R.J., Smith, I.W. and Tyler, R.J. (1973). "Kinetics of Combustion of a Pulverized Brown Coal Char Between 630 and 2200°K". Combustion and Flame, 21, 153-162.

22/ Hughes, P. (1986). Private Communication.

23/ Hagiwara, A., Bortz, S. and Weber, R. (1986). "Theoretical and Experimental Studies on Isothermal, Expanding Swirling Flows with Application to Swirl Birner Design Results of NFA2-1 Investigations", IFRF doc. nr. F259/a/3.

24/ Howard, J.B. (1981) "Fundamental of Coal Pyrolysis and Hydropyrolsis", Chapter 12, Chemistry of Coal Utilization: 2nd Supplementary Volume, Editor M.A. Elliot Wiley-Interscience Publication, New York.

25/ Issa, R.I., (1985). "Solution of Implicitly Discretized Fluid Flow Equations by Operator-Splitting", Dept. of Mineral Resources Engineering, Imperial College, London.

26/ Khalil, K.H., El-Mahallawy, F.M. and Moneib, H.A. (1976). "Effect of Combustion Air Swirl on the Flow Pattern in a Cylindrical Oil Fired Furnace", Combustion, The combustion Institute, p. 135

27/ Lockwood, F.C. and Rizvi, S.M.A. (1983). "Predictive Experience of Coal Firing", Presented at the Meeting on the Combustion of Coal and Other Non-Petroleum Fuel, Central States Section, Lexington, Kentucky.

28/ Lockwood, F.C. and Rizvi, S.M.A., Lee, G.K. and Whaley, H. (1984) "Coal Combustion Model Validation Using Cylindrical Furnace Data", 20th Symposium (Int.) on Combustion, The Combustion Institute.

29/ Lockwood, F.C., Rizvi, S.M.A. and Shah, N.G. (1986), "Comparative Predictive Experience of Coal Firing", Proceeding of Institution of Engineers, vol. 200, NOC2, p 79.

30/ Lockwood, F.C. and Syed, S.A. (1977). "Prediction of Coal Fired Furnaces", Report to CEGB, Imperial College, Mech. Engg. Dept., Techn. Note, FS/78/1.

31/ Launder, B.E., Morse, A.P., Rodi, W. and Spalding, D.B. (1972). "The Prediction of Free Shear Flows - a Comparison of the Performance of Six Turbulence Models", Proc. NASA Conf. on Free Shear Flows, Langley.

32/ Launder, B.E. and Spalding, D.B. (1974). "A Numerical Computation of Turbulent Flows", Computer Methods in Applied Mechanics and Engineering, 3, 269-289.

33/ Launder, B.E. (1978). "Heat and Mass Transport", in "Turbulence", Chapter 6 of Topics in Applied Physics 12 (ed. Bradshaw, P.), Springer.

34/ Lockwood, F.C., Salooja, A.P. and Syed, S.A. (1980). "A Prediction Method for Coal Fired Furnaces", Combustion and Flame: 38, 1-15.

35/ Lockwood, F.C. and Shah, N.G. (1981). "A New Radiation Solution Method for Incorporation in General Combustion Prediction Procedures", 18th Symposium (Int.) on combustion, The combustion Institute.

36/ Migdal, D. and Agosta, V.D. (1976) "A Source Flow Model for Continuous Gas-Particle Flow", Journal of Applied Mechanics, vol. 34, p. 860.

37/ McAskil, D.B. and Hallett, W.L.H. (1984). "Measurements of the flow field in the CCRL Tunnel Furnace at Various Swirl Intensities", CCRL Laboratory CANMET, DSS Contract No. OST84-00015, File No. 24ST. 23440-4-9036, Canada.

38/ Menster, M.H., O'Donnel, H.J., Ergin, S. and Friedell, R.A. (1974). "Rapid Thermal Decomposition of Bituminous Coals", in Coal Classification, Advances in Chemistry Series, No. 131, pp. 1-7, American Chemical Society.

39/ Mulcahy, M.F.R. (1978). "Oxygen in Metal and Gaseous Fuel Industries", p. 175, The Chemical Society, London.

40/ Mulcahy, M.F.R. and Smith, I.W. (1969). Rev. Pur Appl. Chem. 19, 81.

41/ Magnussen, B.F. and Hjertager, B.H. (1976). "Modelling of Turbulent Combustion with Special Emphasis on Soot Formation and Combustion", 16th Symposium (Int.) on Combustion, the Combustion Institute, 719.

42/ Phelan, W.H. and Flament, G. (1982). "The Reduction of NOX Emmissions When Firing a Range of Diverse Coals Using an External Air Stages Burner. Report on the APH Trials", IFRF Doc. Nr. F037/a/12.

43/ Phelan, W.H. and Bontz, S. (1983). "Studies on the Influence of Burner Design Parameters Upon NO Reduction when Staging the Combustion Air with Four Diverse Coals. Report in the AP12 Trials," IFRF doc. nr. F037/a/4.

44/ Patankar, S.V. (1980). "Numerical Heat Transfer and Fluid Flow", Hemisphere Publishing Corporation, Washington.

45/ Pantankar, S.V. and Spalding, D.B. (1972). "A Calculation Procedure for Heat, Mass and Momentum in Three-Dimensional Parabolic Flows", Int. J. Heat Mass Transfer, vol. 15, pp. 1787-1806.

46/ Rizvi, S.M.A., (1985). "Prediction of Flow, Combustion and Heat Transfer in Pulverized Coal Flames", Ph.D. Thesis, University of London.

47/ Rodi, W. (1970). "Basic Equations for Turbulent flow in Cartesian and Cylindrical Co-ordinates", Report No. BL/TN/A/36.

48/ Runchal, A.K., (1972) "Convergence and Accuracy of Three Finite-Difference Schemes and Convection Problem", Int. J. Numerical Methods in Engg., vol, 4, p. 541.

49/ Smith, I.W., (1971). "Kinetics of Combustion of Size-Graded Pulverized Fuels in the Temperature Range 1200-2270°K" Combustion and Flame, 17, 303-314.

50/ Smith, I.W. (1971a). "The Kinetics of Combustion of Pulverized Semi-Anthracite in the Temperature Range 1400-2200°K", Combustion and Flaw, 17, p 421.

51/ Smith, I.W. (1978), "The Intrinsic Reactivity of Carbons to Oxygen", Fuel, 57, p. 409.

52/ Spalding, D.B., (1971). "The Calculations of Combustion Processes", Imperial College, Mech. Engg. Dept., Report RF/TN/A7

53/ Salooja, A.P., (1978). "Mathematical Modelling of an Experimental Study in Axi-symmetrical Combustors", Ph.D. Thesis, University of London.

54/ Smoot, L.D. and Pratt, D.T. (Ed.) (1979). "Pulverized Coal Combustion and "Gasification", Plenum Press, New York.

55/ Smith, I.W. (1982). "The Combustion Rates of Coal Chars: A Review", 19th Symposium (Int.) on Combustion, The Combustion Institute, p. 1045.

56/ Spalding, D.B. (1972). "A Novel Finite-Difference Formulation for Differential Expressions Involving both First and Second Order Derivatives", Int. J. Numerical Methods in Engg., 4, p. 551.

57/ Thring, M.W. and Essenhigh, R.H. (1963). "Chemistry of Coal Utilization". (H.H. lowry Ed.) Suppl. vol. ch. 17, John Wiley, New York.

58/ Wall, T.F. Phelan, W.J. and Bortz, S. (1986). "The Prediction and Scaling of Burn-Out in Swirled Pulverized Coal Flames", IFRF Doc. nr. F388/a/3.

59/ Wallis, G.B. (1969). "One-Dimensional Two-Phase Flow", McGraw-Hill, New York.